

# Chemistry of multiple stellar populations in the mono-metallic, in situ, bulge globular cluster NGC 6388<sup>★ ★★</sup>

Eugenio Carretta<sup>1</sup> and Angela Bragaglia<sup>1</sup>

INAF-Osservatorio di Astrofisica e Scienza dello Spazio di Bologna, Via Gobetti 93/3, I-40129 Bologna, Italy

## ABSTRACT

We present the homogeneous abundance analysis for a combined sample of 185 giants in the bulge globular cluster (GC) NGC 6388. Our results are used to describe the multiple stellar populations and differences or analogies with bulge field stars. Proton-capture elements indicate that a single class of first-generation polluters is sufficient to reproduce both the extreme and intermediate parts of the anti-correlations among light elements O, Na, Mg, and Al, which is at odds with our previous results based on a much smaller sample. The abundance pattern of other species in NGC 6388 closely tracks the trends observed in bulge field stars. In particular, the  $\alpha$ -elements, including Si, rule out an accreted origin for NGC 6388, confirming our previous results based on iron-peak elements, chemo-dynamical analysis, and the age-metallicity relation. The neutron-capture elements are generally uniform, although the [Zr/Fe] ratio shows an intrinsic scatter, correlated to Na and Al abundances. Instead, we do not find enhancement in neutron-capture elements for stars whose photometric properties would classify NGC 6388 as a type II GC. Together with the homogeneity in [Fe/H] we found in a previous paper, this indicates we need to better understand the criteria to separate classes of GCs, coupling photometry, and spectroscopy. These results are based on abundances of 22 species (O, Na, Mg, Al, Si, Ca, Ti, Sc, V, Cr, Mn, Fe, Co, Ni, Zn, Y, Zr, Ba, La, Ce, Nd, and Eu) from UVES spectra sampling proton-,  $\alpha$ -, neutron-capture elements, and Fe-peak elements. For 12 species, we also obtain abundances in a large number of giants (up to 150) from GIRAFFE spectra.

**Key words.** Stars: abundances – Stars: atmospheres – Stars: Population II – Galaxy: globular clusters: general – Galaxy: globular clusters: individual (NGC 6388)

## 1. Introduction

The high-mass, high-metallicity globular cluster (GC) NGC 6388, located in the bulge of the Milky Way (MW) had been poorly studied using high resolution spectroscopy, despite its relevance. The small apparent angular diameter and the large contamination by field stars made it difficult to observe a large number of cluster members (see, e.g. Wallerstein et al. 2007). This has been amended with the use of multi-object spectrographs (such as FLAMES at the ESO VLT; see Carretta et al. 2007a, Lanzoni et al. 2013) and large surveys such as APOGEE (Mészáros et al. 2020: M20). Additionally, a more efficient choice of candidate members can be provided by the *Gaia* mission (see, i.e. the astrometric analysis in Vasiliev and Baumgardt 2021).

This paper presents all the data from our series on NGC 6388 ‘reloaded’, aimed at providing a detailed description of the chemical properties of multiple stellar population in this GC. We started by using the existing data in the ESO archive and added new observations purposely designed to complete the set of setups needed to characterise the chemical composition. In particular, we sought to include all the light elements involved in the (anti-)correlations typical of multiple stellar populations

detected in GCs (Carretta et al. 2009a,b, 2010a, Gratton et al. 2012a, 2019, Bastian and Lardo 2018).

In Carretta and Bragaglia (2018), we analysed UVES spectra of 24 giants (adding 17 new stars to our original set of seven in Carretta et al. 2007a). The resulting pattern of proton-capture elements seemed to imply the necessity of two classes of polluters (the stars that produced the characterising set of light elements in GCs) to explain the anti-correlations between O and Na, Mg, and Al.

The next step (Carretta and Bragaglia 2019) was to discuss the abundance of Mg, Ca, and Sc for the full set of 185 stars observed with both UVES and GIRAFFE. By comparing the abundance ratios in NGC 6388 to those of field stars of similar metallicity, we detected no significant differences for Ca and Sc (at variance with NGC 2808 and a few other massive GCs: see Carretta and Bragaglia 2021), whereas lighter proton-capture species, such as Si, showed clear variations correlated to Mg depletion and Al enhancement. Together with prediction from stellar nucleosynthesis, these observations allowed us to pinpoint the range of internal temperature for the first generation (FG) polluters in NGC 6388 ( $\sim 100 - 150$  MK), with some difference between the cases of the massive stars and asymptotic giant branch (AGB) stars.

We then concentrated on the metal abundance of this cluster and presented (Carretta and Bragaglia 2022a) the atmospheric parameters for our new data set. We also compared our results to literature results and addressed the issue of a metallicity spread. The latter is predicted as a possible property of a separate class of GCs (type II, see below), defined mainly on photometric ground. However, we did not find any significant spread in [Fe/H], not even considering stars belonging to the so-called anomalous red

Send offprint requests to: E. Carretta, eugenio.carretta@inaf.it

<sup>★</sup> Based on observations collected at ESO telescopes under programmes 073.D-0211 and 073.D-0760, 381.D-0329, 095.D-0834, and 099.D-0047.

<sup>★★</sup> Full Tables A.1, A.2, A.3, and A.5 are only available at the CDS via anonymous ftp to cdsarc.u-strasbg.fr (130.79.128.5) or via <http://cdsarc.u-strasbg.fr/viz-bin/cat/J/A+A/??/??>.

giants in the chromosome map, a diagnostic based on Hubble Space Telescope UV photometry used to define the hypothesised class of type II GCs (see Milone et al. 2017). Either an intrinsic spread in iron (and neutron-capture elements, see below) is not a necessary condition to belong to the so-called type II GCs, or NGC 6388 is not a type II GC, as claimed.

Finally, in Carretta and Bragaglia (2022b), we addressed the recent claim that NGC 6388 may have been accreted to the MW, based on the proposed under-abundance of Sc, V, and Zn in four stars (Minelli et al. 2021a). We instead demonstrated how our derived abundances, for a much larger and significant sample of cluster stars, are fully compatible with those of the MW bulge stars and clusters of similar metallicity. Together with chemo-dynamical considerations and the placement of NGC 6388 firmly on the in situ branch of the age-metallicity diagram, our observations conclusively indicate an in situ origin for this GC.

In the present paper, we complete and show the analysis of the dataset, presenting the abundances of 22 species in NGC 6388 from high resolution optical spectroscopy, which permitted a full and homogeneous chemical characterisation of this GC. We discuss our results regarding the multiple stellar population phenomenon, and similarities and differences with the underlying bulge stellar populations.

The paper is organised as follows. A brief summary of data selection and observations is provided in Sect. 2, whereas the abundance analysis and error budget are described in Sect. 3. Results for proton capture and the heavier elements ( $\alpha$ -capture, Fe-peak, and neutron-capture elements) are discussed in Sect. 4 and Sect. 5, respectively. A summary of the properties of NGC 6388 is provided in Sect. 6.

## 2. Summary of data selection and observations

Details on the full procedure we followed to select member stars to be observed in NGC 6388, heavily contaminated by bulge and disc stars, are discussed at length in Carretta and Bragaglia (2022a). We exploited previously made spectroscopic observations (mainly for kinematics) in NGC 6388 to select radial velocity (RV) members. The large value of the systemic RV (80 km s<sup>-1</sup>, Harris 2010) allowed us to individuate bona fide cluster members. Culling our targets from the programmes 073.D-0760 (PI Catelan), 381.D-0329 (PI Lanzoni), and 095.D-0834 (PI Henault-Brunet), we analysed good quality archive data (taken with GIRAFFE high resolution setups HR13 and HR21 or with UVES) or acquired new observations using the same setups (programme 099.D-0047).

Our observing strategy was to obtain GIRAFFE HR13 spectra (to derive atmospheric parameters and abundances of the light elements O, Na, Mg, Si) and HR21 spectra (to derive Al abundances) for as many stars as possible in NGC 6388. Moreover, new UVES/FLAMES spectra were acquired for 12 giants. The new observations were performed from April to August 2017. The wavelength coverage is 6120-6405 Å for HR13, 8484-9001 Å for HR21, and 4800-6800 Å for UVES/FLAMES. The median S/N values are 93, 116, and 50, respectively.

Coordinates, magnitudes, original samples (or new observations), and RVs are listed in Carretta and Bragaglia (2022a) for the 12 and 150 stars with UVES and GIRAFFE spectra, respectively. Similar data for 24 giants with previously analysed UVES/FLAMES spectra can be found in Carretta and Bragaglia (2018).

We consider all stars in our sample to be good candidates as members of NGC 6388 based on the combination of RV and

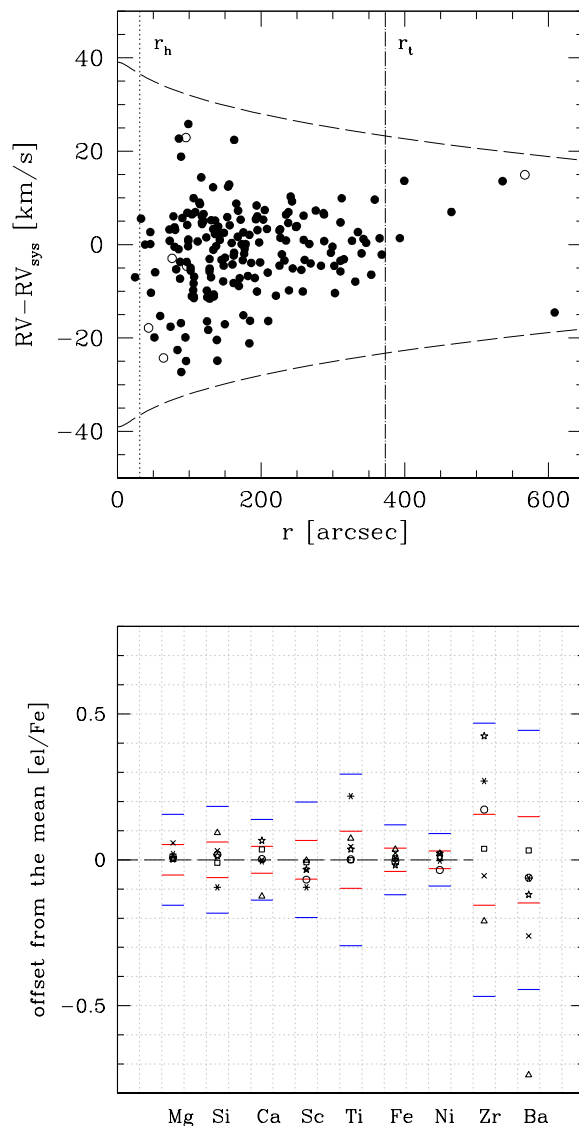


**Fig. 1.** Checks on stars with dubious membership. Upper panel: Radial velocity profile of NGC 6388 based on our sample. The RV refers to the cluster systemic velocity of 82.5 km s<sup>-1</sup>. The open circles indicate stars defined as non-members in APOGEE DR17. The vertical lines indicate the half-mass and tidal radii from Harris (2010). The dashed lines show the  $\pm 3\sigma$  velocity dispersion profile of the best-fit King model as in Lanzoni et al. (2013). All 185 stars fall well inside its limits. Lower panel: For stars in common with APOGEE DR17 and considered non-members there, we show the offsets from the cluster mean elemental ratios ( $[el/Fe]$ ). For each element, the red and blue lines indicate the  $1\sigma$  and  $3\sigma$  limits, respectively. Only the Ba value for star l63p075 is off by more than  $3\sigma$ , and we conservatively excluded this abundance from the computed average in Table 1.

metallicity (presented in previous papers), taking advantage of our derived very small spread in  $[Fe/H]$  (0.04 dex from 185 stars as compared to 0.074 dex from 9 stars in M20). As already discussed in CB22a, for a few stars membership is more dubious because of their proper motions (measured by Gaia) or because they fall outside the tidal radius (if we take the value in Harris 2010, but not if we consider the much larger value in Baumgardt’s database, which would be outside the upper panel

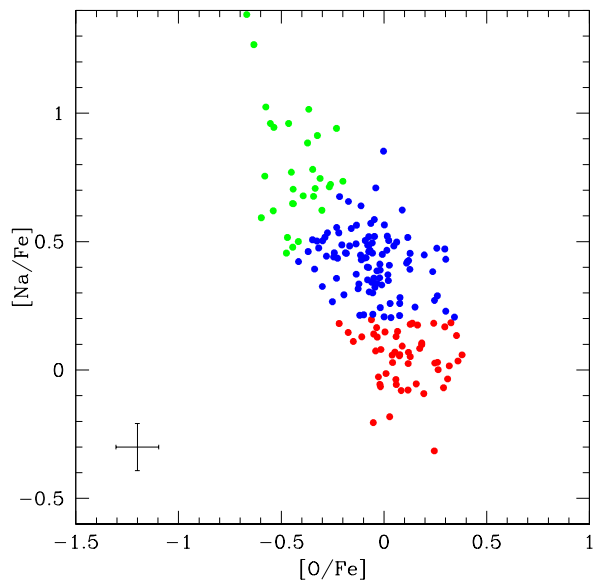


**Fig. 2.**  $[\text{Na}/\text{Fe}]$  abundance ratios as a function of  $[\text{O}/\text{Fe}]$  ratios in NGC 6388. Stars are colour-coded according to their chemical composition following the definitions in Carretta et al. (2009b): red for stars with primordial composition (P), blue for those with intermediate composition (I), and green for stars with heavily altered composition (E). Internal error bars are also reported.

in Fig. 1). Additionally, the referee noted that six of our targets are not considered cluster members in APOGEE DR17. However, as shown in Fig. 1 (upper panel) all stars in our sample fall well within the  $3\sigma$  velocity dispersion profile of the best-fit King model (for details, see Lanzoni et al. 2013, their Fig. 10 and Table 3). Additionally, if we consider the six candidate non-members, we see that the abundances of elements not involved in the multiple populations phenomenon are the same as the bulk of the cluster sample (Fig. 1, lower panel). Furthermore, we find that four of them belong to the second generation, based on their Na and O abundances (see Sect. 4), which decreases the chance of them being field interlopers. In the following, we treat all stars as members, bearing in mind that further studies (e.g. better astrometric data in future Gaia data releases) will help settle the matter.

### 3. Abundance analysis and error budget

The same procedure adopted for GCs previously analysed in our FLAMES survey (see Carretta et al. 2006, 2009a,b) was used here to derive atmospheric parameters and abundances. The metallicity of NGC 6388 is reported and discussed in Carretta and Bragaglia (2022a). As usual, our final effective temperatures  $T_{\text{eff}}$  were derived in two steps. First estimates were obtained from the calibrations of Alonso et al. (1999, 2001). Afterwards, these estimates were refined using a relation between the values from the first step and  $K$  magnitudes of the stars. Surface gravities were then obtained by using the above temperatures, adopting distance modulus  $(m - M)_V = 16.14$  and reddening  $E(B - V) = 0.37$  from Harris (2010), bolometric corrections from Alonso et al. (1999), and masses of  $0.90 M_{\odot}$  and  $M_{\text{bol},\odot} = 4.75$ .

For the abundance analysis we used equivalent widths (EW) measured with the ROSA package (Gratton 1988), after correcting those measured on GIRAFFE spectra to the system given by EWs from UVES spectra. The microturbulent velocities  $v_t$

were derived by minimising the slope of the relation between Fe I abundances and expected line strength (Magain 1984). Models with appropriate atmospheric parameters whose abundances matched those derived from Fe I lines were then interpolated within the Kurucz (1993) grid of model atmospheres. Adopted atmospheric parameters and derived abundances of Fe are listed in Table 2 of Carretta and Bragaglia (2022a). The absence of trends as a function of  $T_{\text{eff}}$  and the good agreement between Fe I and Fe II and between Ti I and Ti II are a good test of the reliability of the adopted scale of atmospheric parameters.

For the other elements, we proceeded as in our FLAMES survey. Oxygen abundances were obtained from the forbidden [O I] line at 6300 Å (more rarely also from the 6363 Å line) after cleaning the telluric lines as described in Carretta et al. (2007a). To correct the Na abundances for non-LTE effects, we adopted the prescriptions from Gratton et al. (1999). Finally, references for the hyperfine structure corrections applied to Sc, V, Mn, and Co can be found in Gratton et al. (2003).

Average abundances are given in Table 1 for the 12 stars observed with UVES and the 150 stars with GIRAFFE spectra. We also list the combination of the abundances of the present sample from UVES with those previously analysed in Carretta and Bragaglia (2018) to show how good the consistency is between the two studies that we merged together. In this table, the neutral species are referred to as Fe I abundances, whereas abundance ratios of ionised species are computed using singly ionised iron. Solar reference abundances are reported in the penultimate column of Table 1, with their sources listed in the last column.

Our procedure to estimate star to star errors due to uncertainties in the adopted atmospheric parameters and in  $EW$  measurements is described in detail in Carretta et al. (2009a) for UVES and Carretta et al. (2009b) for GIRAFFE. For the present work, the outcomes are summarised in Table 2 and Table 3 for abundances obtained from UVES and GIRAFFE spectra, respectively. For the sake of completeness, we also report the values relative to iron in these tables (see Carretta and Bragaglia 2022a, Tables 4 and 5).

We varied one parameter at a time by the amount listed in the first row and repeated the abundance analysis for all stars. The averages provide the sensitivities of abundance ratios to changes in the atmospheric parameters (i.e.  $\Delta[\text{el}/\text{Fe}]/\Delta(\text{par})$ ) and are listed in the main body of the tables. Star-to-star (internal) errors and systematic errors in each parameter are in the second and third rows. The typical internal errors in abundances due to the measurements of EWs (0.02 dex and 0.03 dex for UVES and GIRAFFE, respectively) are estimated as the average rms scatter in Fe abundance divided by the square root of the typical number of measured Fe lines (100 and 20 lines from UVES and GIRAFFE spectra, respectively). Finally, the total internal and systematic errors in the derived abundances are obtained by summing in quadrature the contributions of individual error sources, weighted according to the errors relative to each parameter.

Abundances for individual stars are listed in the Appendix A. For tables containing elements from the whole UVES+GIRAFFE sample, only an excerpt is provided as a guidance of the content. The complete tables can be found at CDS, Strasbourg.

### 4. Proton-capture elements

Sample and observations in NGC 6388 were purposely tailored to measure the largest set of elements involved in proton-capture reactions resulting in the network of correlations and anti-correlations observed in GC stars. Starting from the lightest

**Table 1.** Mean abundances in NGC 6388 for the present and previous samples.

Element	stars	avg	rms	ref	stars	avg	rms	ref	stars	avg	rms	ref	Sun	ref
[Fe/H] <sub>I</sub>	12	-0.509	0.039	(1)	150	-0.488	0.040	(2)	35	-0.480	0.045	(3)	7.54	1
[Fe/H] <sub>II</sub>	12	-0.491	0.039	(1)	149	-0.478	0.053	(2)	35	-0.415	0.081	(3)	7.49	1
[O/Fe] <sub>I</sub>	12	-0.210	0.187	(1)	148	-0.040	0.227	(2)	35	-0.201	0.190	(3)	8.79	1
[Na/Fe] <sub>I</sub>	12	+0.544	0.334	(1)	150	+0.342	0.283	(2)	35	+0.514	0.230	(3)	6.21	1
[Mg/Fe] <sub>I</sub>	12	+0.206	0.043	(1)	149	+0.221	0.052	(2)	35	+0.212	0.049	(3)	7.43	1
[Al/Fe] <sub>I</sub>	12	+0.385	0.391	(1)	125	+0.464	0.303	(2)	35	+0.423	0.350	(3)	6.23	3
[Si/Fe] <sub>I</sub>	11	+0.342	0.029	(1)	150	+0.309	0.061	(2)	34	+0.350	0.063	(3)	7.53	1
[Ca/Fe] <sub>I</sub>	12	+0.082	0.047	(1)	150	+0.069	0.046	(2)	35	+0.062	0.049	(3)	6.27	1
[Sc/Fe] <sub>II</sub>	12	-0.016	0.059	(1)	150	-0.018	0.067	(2)	35	-0.027	0.084	(3)	3.13	1
[Ti/Fe] <sub>I</sub>	12	+0.292	0.050	(1)	150	+0.270	0.098	(2)	35	+0.295	0.086	(3)	5.00	1
[Ti/Fe] <sub>II</sub>	12	+0.282	0.039	(1)					35	+0.244	0.086	(3)	5.07	1
[V/Fe] <sub>I</sub>	12	+0.228	0.103	(1)					35	+0.259	0.143	(3)	3.97	1
[Cr/Fe] <sub>I</sub>	12	-0.138	0.039	(1)					35	-0.104	0.081	(3)	5.67	1
[Mn/Fe] <sub>I</sub>	12	-0.220	0.061	(1)					35	-0.218	0.052	(3)	5.34	1
[Co/Fe] <sub>I</sub>	12	+0.043	0.069	(1)					35	+0.041	0.078	(3)	4.92	2
[Ni/Fe] <sub>I</sub>	12	+0.023	0.022	(1)	150	+0.034	0.030	(2)	35	+0.032	0.029	(3)	6.28	1
[Zn/Fe] <sub>I</sub>	9	+0.128	0.125	(1)					31	+0.102	0.239	(3)	4.59	1
[Y/Fe] <sub>I</sub>	11	-0.323	0.183	(1)					32	-0.259	0.253	(3)	2.24	2
[Zr/Fe] <sub>I</sub>	10	-0.101	0.096	(1)	138	-0.226	0.156	(2)	30	-0.113	0.156	(3)	2.60	2
[Zr/Fe] <sub>II</sub>	10	-0.186	0.203	(1)					29	-0.106	0.181	(3)		
[Ba/Fe] <sub>II</sub>	11	-0.084	0.154	(1)	149	-0.016	0.135	(2)	33	-0.115	0.140	(3)	2.22	3
[La/Fe] <sub>II</sub>	12	+0.155	0.065	(1)					35	+0.191	0.141	(3)	1.22	2
[Ce/Fe] <sub>II</sub>	11	-0.295	0.059	(1)					34	-0.299	0.142	(3)	1.63	3
[Nd/Fe] <sub>II</sub>	11	+0.032	0.082	(1)					34	+0.032	0.091	(3)	1.50	2
[Eu/Fe] <sub>II</sub>	11	+0.253	0.037	(1)					32	+0.248	0.063	(3)	0.55	3

(1) This work; new UVES spectra.

(2) This work; GIRAFFE spectra.

(3) Total sample with UVES spectra (this work + Carretta et al. 2007 + Carretta and Bragaglia 2018).

References for solar: 1=Gratton et al. (2003); 2=Anders and Grevesse (1989); 3=R.Grattton (priv.comm..)]

The average [Ba/Fe] abundance from GIRAFFE is computed by excluding the star l63p075 (see text).

species (O, Na, Table A.1) up to the heavier Ca (Table A.2) and Sc (Table A.3), almost all the interested elements are sampled (potassium is still missing). We also show how, in NGC 6388, these elements define the classical set of anti-correlations and correlations typical of massive GCs, with a couple of notable exceptions that we discuss below.

#### 4.1. The Na-O anti-correlation

The main chemical signature of multiple populations in any GC is evident in Figure 2, where we show the classical anti-correlation between Na and O abundances in 183 stars of NGC 6388. Stars are grouped (and colour-coded) according to their chemical compositions following the PIE scheme as defined in Carretta et al. (2009b). The stars with primordial composition (P, in red in Figure 2) are those with the lowest Na abundances, comprised between  $[\text{Na}/\text{Fe}]_{\text{min}}^1$  ( $= -0.1$  dex) and  $[\text{Na}/\text{Fe}]_{\text{min}} + 0.3$  dex. This choice guarantees the interception of almost the totality of stars with pristine composition, since 0.3 dex is typically a  $3\sigma$  star-to-star error in spectroscopic abundance analysis. The remainder of stars, with chemical compo-

<sup>1</sup> Conservatively, we excluded from this estimate the three stars with the lowest Na values, which seem to be outliers separated from the bulk of stars along the anti-correlation.

sition altered by FG polluters (whatever they were) are dubbed second-generation (SG) stars and divided into two subgroups: those with intermediate composition I (if the ratio  $[\text{O}/\text{Na}] > -0.9$  dex, in blue in Figure 2) and those with extreme E composition ( $[\text{O}/\text{Na}] < -0.9$  dex, green points).

Although more sophisticated methods of statistical cluster analysis (Valle et al. 2021) only retrieve the main blocks of FG and SG stars, our finer separation into I and E stars is not arbitrary, but motivated by the existence of long tails in  $[\text{O}/\text{Na}]$  distributions observed in a number of GCs, such as NGC 2808 and NGC 5904 (M 5) (see Carretta et al. 2009b). In turn, the fractions of stars within each group are correlated to physical properties of GCs, including the total mass (see Table 4 and Figure 14 in Carretta et al. 2010a). We also double checked the PIE attribution using a k-means algorithm. We retrieved three groups almost identical to the ones adopted here, with minor differences at the group edges, corroborating the adoption of the same procedure of all papers of our series on Na-O anti-correlations for the sake of homogeneity.

In the present work, we confirm the fractions we found in Carretta and Bragaglia (2018) for NGC 6388, reducing the associated Poisson errors by half thanks to the much enlarged present sample. A third of stars show a composition with O and Na levels identical to those of field Galactic stars of similar metallicity ( $P=29 \pm 4\%$ ). The remaining SG stars are then split into two

**Table 2.** Sensitivities of abundance ratios to variations in the atmospheric parameters and to errors in the equivalent widths and errors in abundances for stars of NGC 6388 observed with UVES.

Element	Average n. lines	$T_{\text{eff}}$ (K)	$\log g$ (dex)	[A/H] (dex)	$v_t$ kms $^{-1}$	EWs (dex)	Total Internal	Total Systematic
Variation		50	0.20	0.10	0.10			
Internal		6	0.04	0.04	0.12	0.02		
Systematic		17	0.06	0.02	0.04			
[Fe/H] <sub>I</sub>	100	-0.027	+0.041	+0.023	-0.044	0.019	0.058	0.024
[Fe/H] <sub>II</sub>	13	-0.119	+0.122	+0.040	-0.030	0.052	0.072	0.055
[O/Fe] <sub>I</sub>	2	+0.041	+0.038	+0.017	+0.039	0.134	0.142	0.058
[Na/Fe] <sub>I</sub>	4	+0.062	-0.088	+0.017	+0.055	0.095	0.117	0.103
[Mg/Fe] <sub>I</sub>	4	+0.004	-0.027	-0.000	+0.018	0.095	0.097	0.016
[Al/Fe] <sub>I</sub>	2	+0.059	-0.037	-0.018	+0.017	0.134	0.136	0.115
[Si/Fe] <sub>I</sub>	8	-0.043	+0.018	-0.002	+0.026	0.067	0.074	0.020
[Ca/Fe] <sub>I</sub>	16	+0.081	-0.073	-0.009	-0.023	0.047	0.058	0.038
[Sc/Fe] <sub>II</sub>	8	+0.094	-0.034	-0.006	-0.024	0.067	0.074	0.038
[Ti/Fe] <sub>I</sub>	26	+0.104	-0.045	-0.005	-0.035	0.037	0.058	0.042
[Ti/Fe] <sub>II</sub>	11	+0.079	-0.043	-0.008	-0.027	0.057	0.067	0.033
[V/Fe] <sub>I</sub>	12	+0.109	-0.041	+0.003	-0.039	0.055	0.074	0.051
[Cr/Fe] <sub>I</sub>	20	+0.067	-0.043	-0.005	+0.005	0.042	0.044	0.033
[Mn/Fe] <sub>I</sub>	7	+0.045	-0.030	+0.009	-0.011	0.071	0.073	0.025
[Co/Fe] <sub>I</sub>	5	-0.001	+0.006	-0.002	-0.009	0.085	0.085	0.020
[Ni/Fe] <sub>I</sub>	36	-0.005	+0.015	+0.003	+0.008	0.032	0.033	0.008
[Zn/Fe] <sub>I</sub>	1	-0.035	+0.006	-0.005	-0.013	0.189	0.190	0.044
[Y/Fe] <sub>I</sub>	2	+0.122	-0.023	-0.005	-0.012	0.134	0.135	0.069
[Zr/Fe] <sub>I</sub>	5	+0.105	-0.012	-0.001	-0.006	0.085	0.086	0.046
[Zr/Fe] <sub>II</sub>	1	+0.089	-0.034	-0.003	+0.015	0.189	0.190	0.060
[Ba/Fe] <sub>II</sub>	3	+0.126	-0.062	+0.006	-0.056	0.109	0.130	0.054
[La/Fe] <sub>II</sub>	2	+0.128	-0.043	-0.002	-0.029	0.134	0.139	0.050
[Ce/Fe] <sub>II</sub>	1	+0.122	-0.049	-0.005	-0.001	0.189	0.190	0.047
[Nd/Fe] <sub>II</sub>	5	+0.122	-0.045	-0.004	-0.026	0.085	0.092	0.049
[Eu/Fe] <sub>II</sub>	2	+0.109	-0.044	-0.004	+0.013	0.134	0.135	0.041

**Table 3.** Sensitivities of abundance ratios to variations in the atmospheric parameters and to errors in the equivalent widths and errors in abundances for stars of NGC 6388 observed with GIRAFFE.

Element	Average n. lines	$T_{\text{eff}}$ (K)	$\log g$ (dex)	[A/H] (dex)	$v_t$ kms $^{-1}$	EWs (dex)	Total Internal	Total Systematic
Variation		50	0.20	0.10	0.10			
Internal		6	0.04	0.04	0.22	0.03		
Systematic		57	0.06	0.02	0.01			
[Fe/H] <sub>I</sub>	20	+0.014	+0.032	+0.022	-0.060	0.027	0.067	0.020
[Fe/H] <sub>II</sub>	3	-0.079	+0.118	+0.040	-0.018	0.070	0.079	0.097
[O/Fe] <sub>I</sub>	2	-0.001	+0.049	+0.017	+0.057	0.086	0.104	0.025
[Na/Fe] <sub>I</sub>	2	+0.025	-0.054	-0.009	+0.031	0.086	0.092	0.040
[Mg/Fe] <sub>I</sub>	2	-0.015	-0.009	-0.012	+0.050	0.086	0.100	0.018
[Al/Fe] <sub>I</sub>	2	+0.016	-0.054	-0.020	+0.033	0.086	0.093	0.037
[Si/Fe] <sub>I</sub>	3	-0.056	+0.014	+0.001	+0.047	0.070	0.085	0.064
[Ca/Fe] <sub>I</sub>	5	+0.048	-0.064	-0.016	+0.007	0.055	0.057	0.058
[Sc/Fe] <sub>II</sub>	2	+0.068	-0.033	-0.005	-0.015	0.086	0.088	0.078
[Ti/Fe] <sub>I</sub>	3	+0.069	-0.035	-0.019	-0.019	0.070	0.074	0.080
[Ni/Fe] <sub>I</sub>	11	-0.022	+0.019	+0.001	+0.035	0.037	0.051	0.026
[Zr/Fe] <sub>I</sub>	4	+0.084	-0.020	-0.019	+0.037	0.061	0.073	0.097
[Ba/Fe] <sub>II</sub>	1	+0.090	-0.067	+0.005	-0.060	0.122	0.137	0.105

components, the bulk consisting of stars with intermediate composition ( $I=54 \pm 5\%$ ). Finally, we confirm once again that in NGC 6388 there is a noticeable fraction of stars showing an extremely modified composition ( $E=16 \pm 3\%$ ). These computations are made over 184 stars, because although two stars are lacking O abundances, one of them (163p307) has  $[\text{Na}/\text{Fe}] = +0.102$  dex, a value that firmly places it in the P population.

The fraction E also includes the two stars with the highest Na abundances ( $[\text{Na}/\text{Fe}] > 1.2$  dex). They are members of NGC 6388 according to both the RV and metallicity measured on our spectra and *Gaia* astrometry (Vasiliev and Baumgardt 2021). They lie nicely on the locus of the Na-O anti-correlation and are also the stars with the lowest O abundances in our sample ( $[\text{O}/\text{Fe}] < -0.6$  dex, see Table A.1). We note that even if all the

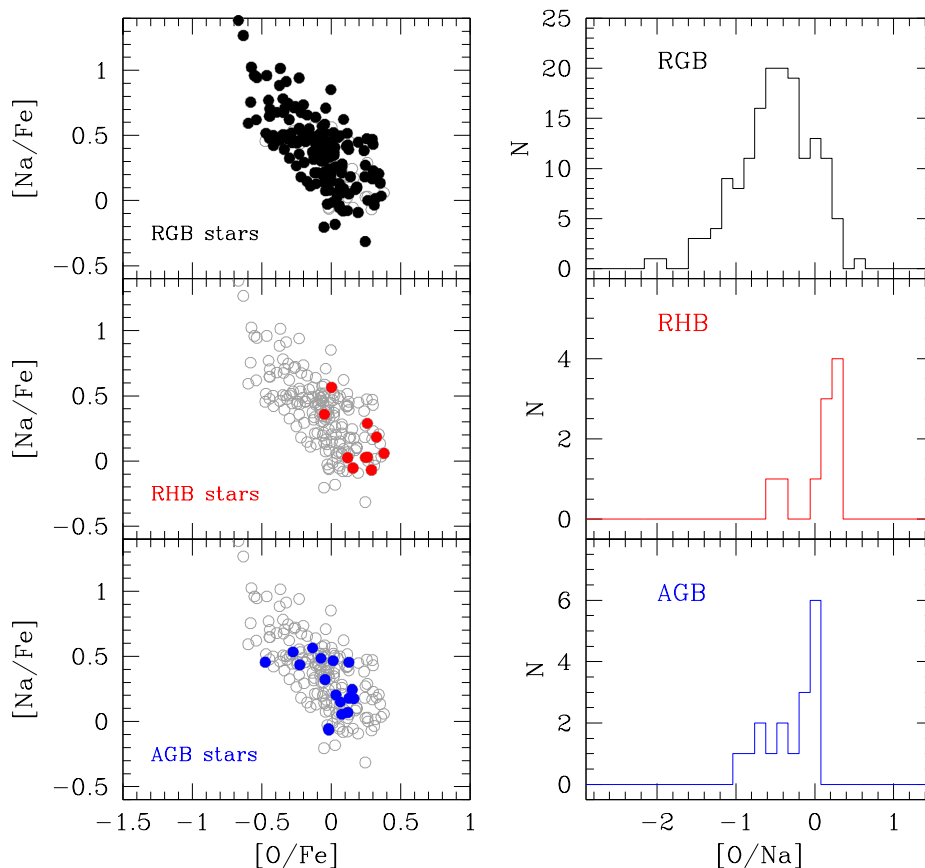


**Fig. 3.** Anti-correlation of Na and O abundances in stars of NGC 6388 in different evolutionary phases. In all three panels on the left, open circles are our total sample. In the top left panel, we plot RGB stars as filled circles. In the middle and lower panels, we superimpose values for RHB and AGB stars, in red and blue filled circles, respectively. In the right column, we show the observed distributions of the  $[O/Na]$  abundance ratios for RGB, RHB, and AGB stars, from top to bottom, respectively.

six stars flagged as possible non-members in APOGEE DR17 were excluded, our results on multiple stellar populations and their respective composition in NGC 6388 would not change. Their exclusion would only change the fraction of P, I, and E stars within their associated Poissonian errors.

Formally, we observe a monotonic increase of the metal abundance along the sequence PIE. The average  $[Fe/H]$  of the three groups raises from  $-0.493$  dex for 55 P stars to  $-0.485$  dex and  $-0.481$  dex for I (100 objects) and E stars (30 objects), respectively. Although statistically not significant, this progression is what is expected following an increasing helium abundance in SG stars of the I and E groups. The effect is to increase the strength of metallic lines (see Böhm-Vitense 1979), and that of neutral lines more than that of ionised lines. This is clearly confirmed by the iron difference between P and E stars, which we find to be 0.006 dex for Fe II, half of that derived from Fe I lines. Although the combination of tiny differences in abundance between the groups and internal errors associated with iron prevents a stronger statement, these results qualitatively conform to expectations.

#### 4.2. Horizontal and asymptotic giant branch stars

Our sample in NGC 6388 includes a small number of stars that are not on their first ascent on the red giant branch (RGB), since

our selection criterion for membership was exclusively based on RVs (see Sect.2). This provides the opportunity to homogeneously compare the behaviour of multiple stellar populations in different evolutionary phases. The main spectroscopic feature, the anti-correlation of Na-O abundances, is examined in Fig. 3. In the panels of the left column, we highlight the abundances of ten red HB stars (RHB, red filled circles) and 17 asymptotic giant branch stars (AGB, blue filled circles) on the overall Na-O anti-correlation obtained for the whole sample. While there are no differences in the metal abundances (the average  $[Fe/H]$  values agree within 0.003 dex), as expected, the different patterns for proton-capture species are evident.

Also this second finding is hardly surprising. At odds with the PIE classification of RGB stars (fractions 25, 56, and 19%, respectively), when we only consider RHB stars we find that the vast majority (70%) are in the P component, with only 30% falling in the I group of SG stars (just the reverse proportion with respect to RGB stars). Moreover, no RHB star is found with the highly modified composition typical of the E component.

Our findings agree with the well-known scenario where stars with different He contents are located on distinct portions of the HB. Spectroscopic detections of He in HB stars are hard to obtain, but since He variations are correlated to star to star abundance variations in light elements (see Gratton et al. 2004, 2012a, 2019; Bastian and Lardo 2018) it is much easier to prove



this scenario by analysing the pattern of other elements, including Na and O (see Gratton et al. 2011, 2012b, 2013, 2014, 2015, Villanova et al. 2009, 2012, Marino et al. 2011a). The almost complete segregation of Na-poor/O-rich stars on the red extreme of the HB is a natural consequence of the strong correlation linking the chemical variations in proton-capture species in GC stars and the highest temperature that may be reached on the ZAHB in each GC, as found by Carretta et al. (2007b). In turn, these observations agree with the prediction by D’Antona et al. (2002) that variations in helium (or their proxies, variations in light elements) are a key ingredient to explain the HB morphology. In NGC 6388, all the analysed HB stars belong to the RHB, so they behave almost like a simple stellar population, with the  $[O/Na]$  ratio peaking at a high value (see Fig. 3, right column, middle panel).

The lower panels in Fig. 3 show the situation for the 17 AGB stars in our sample. They are 11% of the RGB stars in our sample, so we are confident that we did not miss a significant fraction of objects in this evolutionary phase, since AGB stars are rarer (see discussion in Gratton et al. 2010 and their Table 1). From the lower left panel in Fig. 3 and the number counts, we see that the fraction of SG stars with intermediate composition (the I component) is similar in RGB and AGB stars (56% and 53%, respectively). The largest differences are for the primordial P component (25% for RGB and 41% for AGB stars) and, in particular, for the extreme E component with only one AGB star classified as such (18% for RGB and 6% for AGB stars). This agrees with previous findings. Gratton et al. (2010) discussed the well-established lack of CN-strong objects among AGB stars in GCs (e.g. Norris et al. 1981, Campbell et al. 2010) and correlated it with the HB properties, in particular with the expectation that the less massive HB stars do not even begin their AGB phase (AGB manqué). That means that the most He-rich (Na-rich and O-poor) stars in GCs, those we would classify as E, do not reach the AGB. More recent results, sometimes contradictory, and further discussions on the different fractions of FG and SG in RGB and AGB stars can be found, for instance, in Marino et al. (2017), Wang et al. (2017), and MacLean et al. (2018).

Although the distributions of both RHB and AGB stars peak at higher values than RGB stars (right column in Fig. 3), the average  $[O/Na]$  for AGB stars is shifted to a lower value than for RHB stars. A look at the panels in the left column shows that the effect is not due to different Na abundances (mean  $[Na/Fe]=+0.141$  rms=0.205 dex in RHB and  $+0.275$  rms=0.206 dex in AGB), but rather to an actual difference in the average O content (mean  $[O/Fe]=+0.199$  rms=0.140 dex in RHB and  $-0.023$  rms=0.173 dex in AGB). We used Student’s and Welch’s tests with the null hypothesis that the groups of RHB and AGB stars are extracted from a distribution with the same means. This hypothesis cannot be rejected in the case of Na (two-tail probability  $p = 0.114$ , 25 d.o.f.), whereas it can be safely rejected regarding the  $[O/Fe]$  average content ( $p = 1.2 \times 10^{-3}$ ), confirming that we are probably observing a real difference. The above discussion also confirms well-known behaviours in NGC 6388 due to the global multiple population phenomenon, without the need to invoke systematic or model-dependent effects.

A further difference concerns the radial distribution of stars in different evolutionary phases. In Fig. 4, we plot the cumulative distributions of radial distances for stars in our sample, together with the results of a Kolmogorov-Smirnov test to ascertain statistical differences between different groups. We find that RHB stars are more externally distributed in the GC than both RGB and AGB stars. Due to the limited size of the RHB and AGB samples, we prefer not to expand further on this. On the other

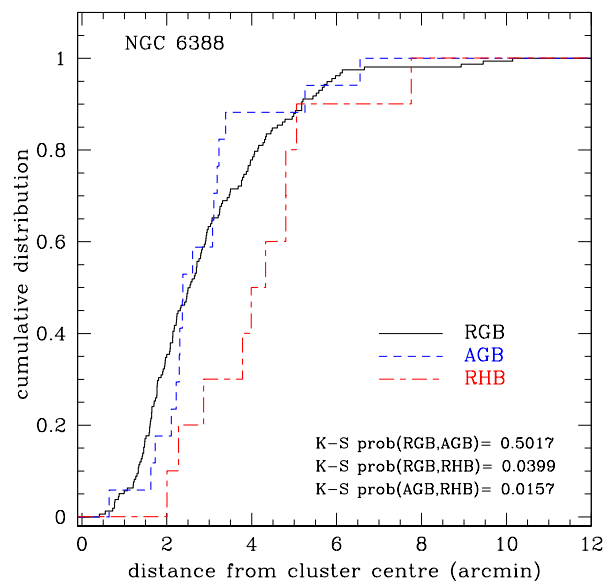


**Fig. 4.** Cumulative distributions of radial distances for stars in NGC 6388 in different evolutionary phases: RGB (black solid line), RHB (red short-long dashed line), and AGB (blue dashed line). The probabilities of the Kolmogorov-Smirnov test are labelled in the panel.

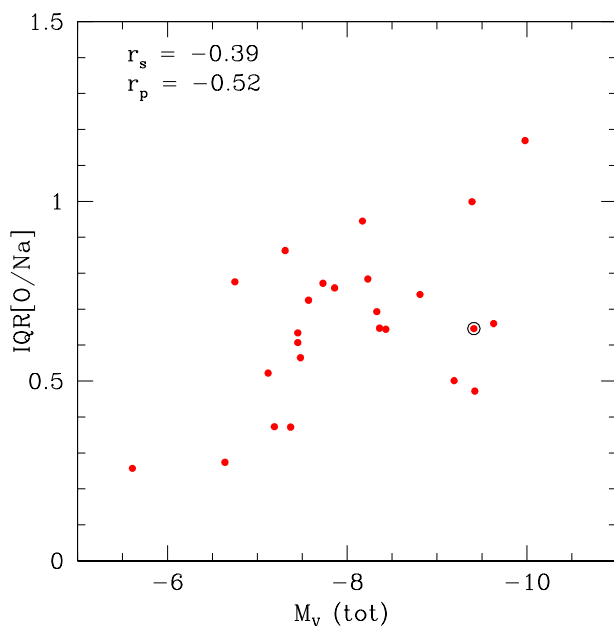


**Fig. 5.** Extension of Na-O anti-correlation in 25 GCs of our FLAMES survey as measured by the inter-quartile range of the  $[O/Na]$  ratio, as a function of the total mass (using the total cluster absolute magnitude as proxy). NGC 6388 is indicated with an open circle.

hand, we do not find any relevant difference in the concentration of stars in the P, I, and E groups.

#### 4.3. The peculiar Na-O anti-correlation of NGC 6388

The inter-quartile range of the  $[O/Na]$  ratio was proposed by Carretta (2006) as a robust estimate of the extension of the Na-O anti-correlation because it is more insensitive to outliers than other traditional indicators (e.g. the intrinsic spread as measured

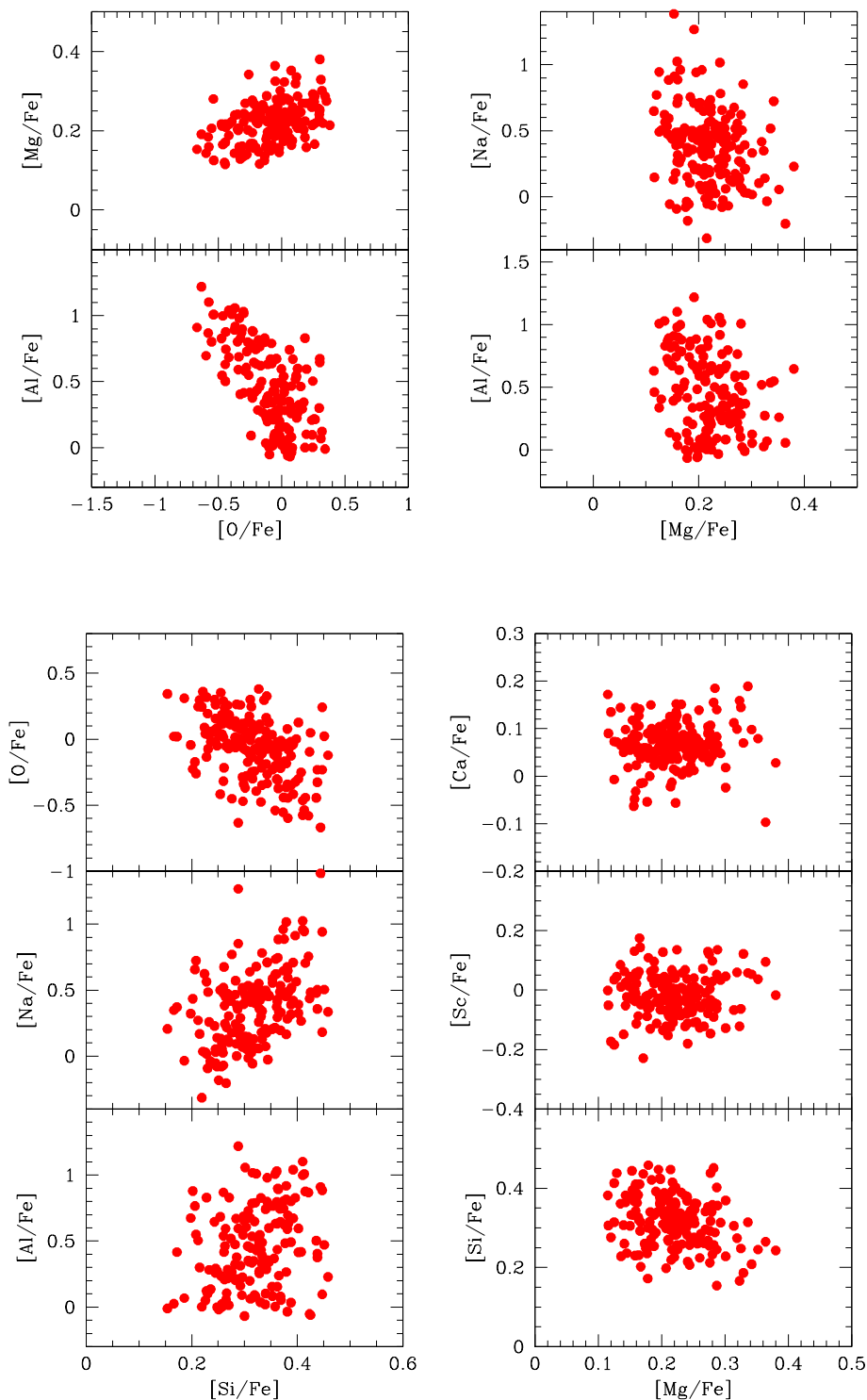


**Fig. 6.** Mutual correlations and anti-correlations among proton-capture elements in stars of NGC 6388. Internal, star to star errors can be found in Table 2 and Table 3.

by the rms scatter). From the 183 stars in NGC 6388 with measured O and Na abundances, we obtained  $\text{IQR}[\text{O}/\text{Na}] = 0.638$ , which agrees with the previous value (0.644) derived from a sample of only 49 stars in Carretta and Bragaglia (2018). We then confirm that NGC 6388 belongs to the group of massive GCs whose extent of the Na-O anti-correlation is too short with respect to what expected on the basis of their total mass. In Fig. 5, we show the  $\text{IQR}[\text{O}/\text{Na}]$ -mass relation from our

FLAMES survey (see Carretta et al. 2010a), where we adopt the cluster total absolute magnitude  $M_V$  as a model-independent proxy of the present-day GC total mass. When we plot the 25 GCs of our FLAMES survey homogeneously analysed, we note that NGC 6388 falls in a group of four GCs standing out of the main trend, the other ones being NGC 6441, NGC 104 (47 Tuc), and NGC 7078 (M 15).



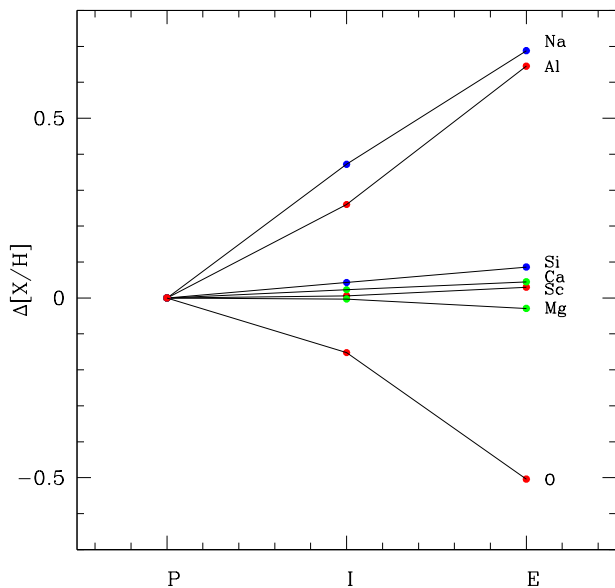


**Fig. 7.** Run of different element abundances among PIE groups in NGC 6388, indicated by the average differences with respect to the P group, whose composition is representative of the primordial abundances in the proto-GC.

This behaviour is not dependent on our abundance analysis, since it is confirmed by literature data such as 104 giants for NGC 104 (Cordero et al. 2014) or 18 giants in M 15 (Snedden et al. 1997). At present, we have no explanation for these four GCs having an extension shorter than expected for the Na-O anti-correlation, given their rather large total mass.

#### 4.4. The other proton-capture elements

We determined the abundances of other elements (Mg, Al, Si, Ca, and Sc) involved in the network of proton-capture reactions acting to modify the primordial chemical composition of GC stars. The mutual relations among these species in NGC 6388 are illustrated in Fig. 6. Internal errors can be found in Table 2 and Table 3.

The trends visible in this figure point out once again that the whole pattern we see among light elements in GC stars is clearly due to some form of nucleosynthesis, because the variations in the chemical composition are not randomly distributed, but follow well-known evolutions. There could be some residual uncertainties related to the statistical grouping of stars, but the three stellar populations are consistently ordered according to all abundances. Enhancement in Al is accompanied by a depletion in Mg, Na is lower when O is higher, and so on.

These trends are well summarised in Fig. 7, where we represent the average abundances of different elements in the three components P, I, and E in NGC 6388. In this figure, we plot the average differences with respect to the P group, so that the trends are a direct representation of the changes in the chemical composition due to the formation of multiple populations with respect to the floor of primordial abundances in the proto-GC.

Not surprisingly, we retrieve the large enhancements in Na and Al contents, paralleled by a noticeable O depletion, and a smaller decrease in Mg abundance. Both the Si-Al correlation and the Mg-Si anti-correlation act as a precision thermometer that probes the inner temperature reached by the FG polluters.

**Table 4.** Tests on (anti-)correlations.

rel.	$r_s$ Spearman.	$r_p$ Pearson	Nr. stars	t Stud.	prob. two-tails
Al-O	-0.602	-0.638	160	9.477	$< 1.0 \times 10^{-6}$
Na-O	-0.676	-0.693	183	12.342	$< 1.0 \times 10^{-6}$
Na-Mg	-0.242	-0.267	184	3.738	$2.5 \times 10^{-4}$
Na-Al	+0.691	+0.704	160	12.460	$< 1.0 \times 10^{-6}$
Na-Si	+0.443	+0.443	184	6.666	$< 1.0 \times 10^{-6}$
Al-Mg	-0.255	-0.264	160	3.440	$7.4 \times 10^{-4}$
Si-Mg	-0.286	-0.305	183	4.309	$2.7 \times 10^{-5}$
Si-Al	+0.275	+0.266	159	3.458	$7.0 \times 10^{-4}$
O-Si	-0.479	-0.468	182	7.105	$< 1.0 \times 10^{-6}$
O-Mg	+0.397	+0.402	182	5.890	$< 1.0 \times 10^{-6}$
Ca-Mg	+0.032	+0.041	184	0.554	0.581
Sc-Mg	-0.067	+0.024	184	0.324	0.746

The small but steady increase in the [Si/Fe] ratio when progressing from P to I and to E component (and the simultaneous decrease in [Mg/Fe]) has been explained (e.g. Karakas and Lattanzio 2003; Yong et al. 2005) by the leakage from the Mg-Al cycle on  $^{28}\text{Si}$ . This occurs when the two reactions  $^{27}\text{Al}(p,\gamma)^{28}\text{Si}$  and  $^{27}\text{Al}(p,\alpha)^{24}\text{Mg}$  switch as relevance at a well-defined temperature of  $\sim 65$  MK (see Arnould et al. 1999, their Figure 8). Concerning NGC 6388, this means that whatever the polluters were, in the early evolution of the primordial population of the cluster they were able to reach such a temperature.

In Carretta and Bragaglia (2019), we investigated the high extreme of the temperature range possibly reached by the FG polluters in order to reproduce the pattern of heavier proton-capture species, such as Sc and Ca. The idea was to ascertain in NGC 6388 the presence (or lack) of the anti-correlations found between the abundances of both Sc and Ca with those of Mg in the massive cluster NGC 2808 (Carretta 2015). Their existence in NGC 2808 was interpreted in the same framework of proton-capture reactions at very high temperature used by Ventura et al. (2012) to explain the unique pattern of the K-Mg anti-correlation in NGC 2419 (see Cohen and Kirby 2012, Mucciarelli et al. 2012). The variations of Sc and Ca in NGC 2808 and the anti-correlation K-Mg, later found by Mucciarelli et al. (2015), showed that this extreme regime of H-burning can be traced even in more normal GCs than NGC 2419. However, in Carretta and Bragaglia (2019) we were able to show that the abundances of Sc and Ca in NGC 6388 cannot be distinguished from those of field stars of similar metallicity. The latter represent fairly well the unpolluted, primordial population of stars where only the effects of supernova nucleosynthesis can be tracked. In turn, these observations mean that the FG polluters in NGC 6388 were not able to reach the temperature of about 150 MK, above which seed species including Ar and K start to be affected, allowing the production of elements such as Sc and Ca (see Prantzos et al. 2017). The constraints from the Si Al variations and the evidence of Sc and Ca being largely unaffected would pinpoint a narrower range of 100-120 MK for the temperature reached in the candidate polluters if these can be identified with massive AGB stars (see D'Antona et al. 2016). In Fig. 7, we note a slight enhancement in Sc and Ca in the extreme E fraction of stars in NGC 6388, but it is not significant.

The scenario and the conclusions discussed above strongly support statistics as shown in Table 4, where we list the parameters of linear regressions through the different relations among light elements shown in Fig. 2 and Fig. 6. We tested the level

of significance for each regression, reporting the results in the last two columns of Table 4. The two-tail probabilities listed show that all the relations involving O, Na, Mg, Al, and Si in NGC 6388 are real with a high level of significance. On the contrary, the two anti-correlations between Mg and Sc, and Mg and Ca are not significant. We can then confirm, based on robust evidence, that in NGC 6388 the FG polluters, whatever they were, likely reached a maximum inner temperature restricted to a narrow range between 100 and 120-150 MK, as found in Carretta and Bragaglia (2019).

#### 4.5. Light elements, polluters, and dilution

In Carretta and Bragaglia (2018), we tried to ascertain how many classes or kinds of polluters may have been contributing to the chemical budget of NGC 6388. We performed this exercise using the same approach adopted in Carretta et al. (2012) to study the discrete components in NGC 6752.

We started with the simple dilution model (illustrated, e.g. in Carretta et al. 2009b), where we reproduce the chemical pattern of the various stellar populations by mixing the composition of the E group with different fractions of primordial gas, which is simply represented by the composition of the P component. This means that the I population would be obtained by mixing a fraction  $dil$  of matter with E-like composition together with a fraction whose composition is P-like. It follows that if only a class of polluters was in action, then the value of  $dil$  should be the same for all elements:

$$dil = \frac{[A(X)_I - A(X)_P]}{[A(X)_E - A(X)_P]} = \frac{[A(Y)_I - A(Y)_P]}{[A(Y)_E - A(Y)_P]}, \quad (1)$$

where  $A(X)$  and  $A(Y)$  are the abundances in number of atoms of elements X and Y.

The results reached in Carretta and Bragaglia (2018) were not conclusive. The main obstacle was the availability of Al abundances only for the limited sample of 24 stars with UVES spectra. In turn, this provided two different possible divisions in the P, I, and E groups, depending on whether the groups were based on the Al-O or the Na-O plane. As a consequence, we cannot not entirely exclude the possibility that more than a single class of polluters could be necessary to produce the observed composition of the I component.

With the present large sample of stars for which homogeneous abundances of several proton-capture species are obtained in NGC 6388, this problem is solved. For instance, our sample of stars with derived Al abundances is increased by a factor 6.7, with respect to Carretta and Bragaglia (2018). Thus, we repeated the exercise.

We found that in the chemical planes Al-O, Na-O, Al-Mg, and Si-Mg a simple dilution model, anchored to the mean values for P and E stars, now nicely passes through the average value of the intermediate I population, as shown in Fig. 8 and at variance with what was found in Carretta and Bragaglia (2018). We thus conclude that the hints of multiple classes of polluters seen in Carretta and Bragaglia (2018) were likely due to the limited size of the available samples (especially Al abundances). Our present results are compatible with the existence of a single class of FG polluters able to reproduce the observed characteristics of multiple stellar populations in NGC 6388, when their ejecta were mixed with variable amount of pristine gas.

A summary of the above exercise is given in Fig. 9, where we plot the resulting dilution factors  $dil$  for each considered species (indicated by the atomic number). The value corresponding to

Mg is indicated with a different symbol (empty circle) to stress the large associated error. The same behaviour was already noted in Carretta and Bragaglia (2018) and tentatively attributed to the small variations in the abundance of Mg with respect to the primordial value. However, we note that star-to-star variations in the Si content are also small, yet its derived dilution factor is compatible with the others species. At present, we do not have a satisfactory explanation for the behaviour of the dilution of Mg.

The values we found for  $dil$  are  $0.41 \pm 0.09$ ,  $0.30 \pm 0.06$ ,  $0.14 \pm 0.38$ ,  $0.30 \pm 0.06$ , and  $0.48 \pm 0.16$  for O, Na, Mg, Al, and Si, respectively. Apart from Mg, all these values lie within  $\pm 1\sigma$  from the average values labelled in Fig. 9, a strong indication for a unique class of polluters acting in NGC 6388.

## 5. The chemical composition of NGC 6388 in context

### 5.1. $\alpha$ -capture elements

Thanks to the spectral range of UVES spectra and to the large size of our overall dataset, we were able to analyse the full set of  $\alpha$ -elements in NGC 6388 for a large number of stars. Both products of hydrostatic burning (O, Mg) and explosive nucleosynthesis (Si, Ca, Ti) were analysed. Their run as a function of the effective temperature is summarised in Fig. 10 (red and blue points for stars with GIRAFFE and UVES spectra, respectively). Internal error bars for this figure are listed in Table 2 and Table 3 for abundances derived from UVES and GIRAFFE spectra, respectively. No dependence of abundance on  $T_{\text{eff}}$  is present for any of these elements, over a range of luminosity of more than four magnitudes.

Since the key work by Tinsley (1979), abundance ratios were used as probe of the birth properties of stars. The interplay between star formation and stellar lifetimes (driven by the mass) means that elements from different nucleosynthetic sites can be combined into abundance ratios useful to uncover the primordial environment where the observed stars were born. In particular, the  $\alpha$ -Fe plane is a privileged indicator, since a similarity in this plane for two stellar populations indicates a similar chemical evolution of the systems. However, the metallicity at which the so-called knee due to the onset of Type Ia SNe occurs depends on the system's stellar mass and on the efficiency of star formation in the progenitor galaxy (see, e.g. the review by Tolstoy et al. 2009). Owing to the impact of these abundance patterns on the clues for the origin of NGC 6388, our results on  $\alpha$ -elements deserve a detailed discussion.

The average amount of  $\alpha$ -elements in NGC 6388 is overabundant with respect to the solar level, which is compatible with a chemical composition dominated by the contribution of type II SNe acting before a significant number of SN Ia started to add increasing amounts of iron and lower the ratio  $[\alpha/\text{Fe}]$ . This evidence, together with the time delay expected for the bulk explosions of SN Ia, is also consistent with GCs in the bulge being old and nearly coeval to halo GCs, with similar levels of  $\alpha$ -element overabundance.

The average  $[\text{Si}/\text{Fe}]$  ratio reflects the typical overabundance with respect to the solar values found also in the majority of GCs and for the other  $\alpha$ -elements in Fig. 10. We found a mean  $[\text{Si}/\text{Fe}]$  of 0.31 dex from 150 stars with GIRAFFE spectra and 0.35 dex from 34 stars observed with UVES, after combining the results for the 12 new stars of the present study with the sample analysed in Carretta and Bragaglia (2018). We thus confirm the high value we found in our first analysis for NGC 6388 (Carretta et al. 2007a), which is at odds with the low values derived by

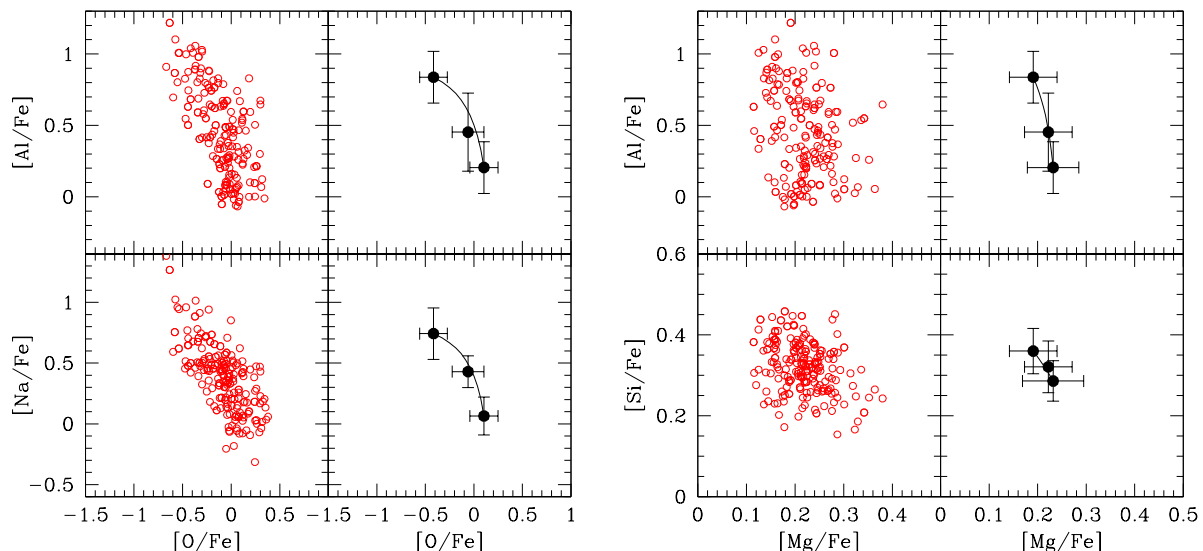


**Fig. 8.** Observed Al-O, Na-O, Al-Mg, and Si-Mg anti-correlations in NGC 6388 (empty red circles). Black filled points are the average values of each element in the P, I, E groups. Solid lines are a simple dilution model anchored to the primordial P and extreme E components.

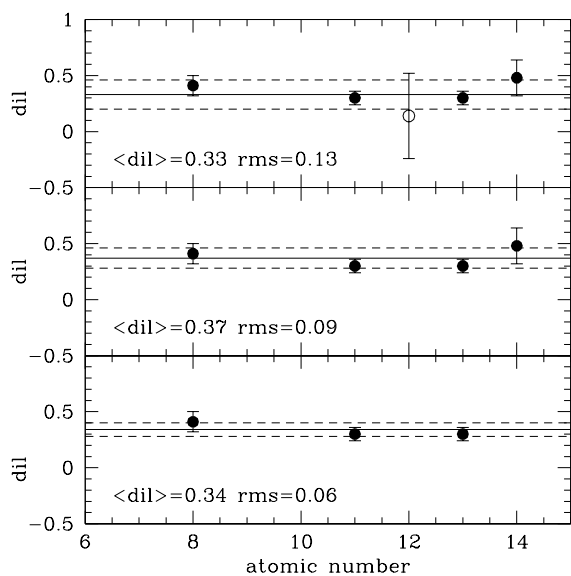


**Fig. 9.** Summary of the dilution factors for different elements (indicated by the atomic number). In the three panels we indicate the average values (solid lines) and the associated  $\pm 1\sigma$  (dashed line) resulting: i) from all the five considered species, ii) neglecting Mg (empty symbol with large error bar), and iii) considering only O, Na, and Al, (from top to bottom, respectively).

the APOGEE DR16 ( $\langle [\text{Si}/\text{Fe}] \rangle = -0.03 \pm 0.1$  dex, as reported in Horta et al. 2020) and DR17 ( $\langle [\text{Si}/\text{Fe}] \rangle = +0.045 \pm 0.061$  dex), from 53 stars flagged as members of NGC 6388 (Abdurro'uf et al. 2022).

Conversely, in NGC 6388 we found a value ( $\sim 0.07$  dex, see Table 1) for the average  $[\text{Ca}/\text{Fe}]$  ratio lower than for other  $\alpha$ -elements. However, this is fully consistent with our previous analyses (Carretta et al. 2007a, Carretta and Bragaglia 2018). Gratton et al. (2006) observed a similarly low value in the massive bulge cluster NGC 6441, and they advanced the hypothesis

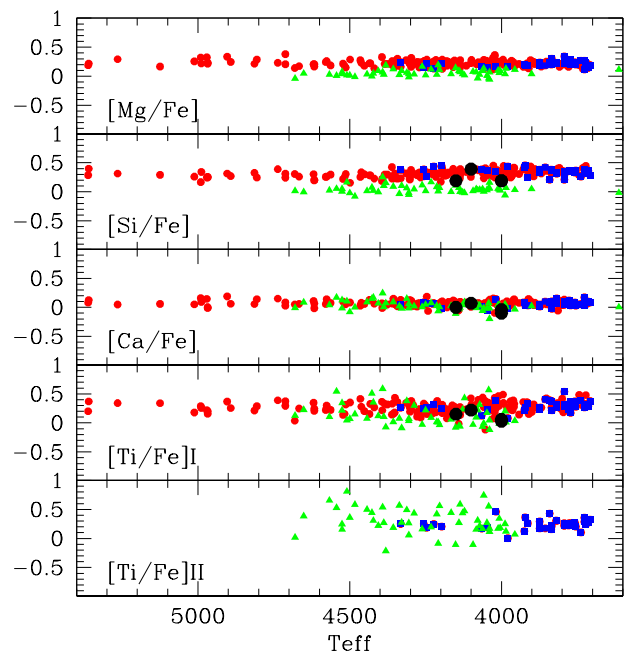


**Fig. 10.** Abundance ratios  $[\text{Mg}/\text{Fe}]$ ,  $[\text{Si}/\text{Fe}]$ ,  $[\text{Ca}/\text{Fe}]$ ,  $[\text{Ti}/\text{Fe}]_{\text{I}}$ , and  $[\text{Ti}/\text{Fe}]_{\text{II}}$  for stars in NGC 6388 as a function of the effective temperature. For the present work, red filled circles indicate stars with GI-RAFFE spectra, whereas stars with UVES spectra are represented with blue filled squares. Large black circles indicate the four stars analysed by Minelli et al. (2021a), and green filled triangles are stars in APOGEE DR17 flagged as members of NGC 6388.

that this deficiency in Ca could be an artefact of the analysis, due to using strong lines in bright and cool giants. However, this explanation hardly applies to our sample, which includes stars spanning a range of about 1700 K in  $T_{\text{eff}}$ .

A comparison of the abundance of  $\alpha$ -elements in NGC 6388 from both optical and infrared studies is provided in Fig. 10.

To our derived abundances we superimposed the four stars re-analysed by Minelli et al. (2021a) (large black circles) and the about 50 stars flagged as members of NGC 6388 in the APOGEE DR17 (filled green triangles). Looking at this Figure, clear offsets are present between the abundances from infrared and optical spectra, with both optical analyses giving consistent results (at least for the  $\alpha$ -elements, see Carretta and Bragaglia 2022b and the next section). In particular, Mg and Si abundances from APOGEE are lower than we find here, whereas a good agreement is found for Ca abundances. For Ti, we are instead seeing a larger spread in APOGEE abundances.

Part of the offsets may be explained by differences in the adopted solar reference abundances. They are not given in the DR17 paper, but assuming that they are not changed from DR16, we used the solar values provided by Smith et al. (2021) for DR16 to compute the corrections needed to bring infrared data on our solar scale (respectively +0.19, +0.11, +0.13, and -0.01 dex for Mg, Si, Ca, and Ti). The overall agreement would improve for Mg and Si, but it would worsen for Ca.

For a more quantitative comparison, in Table 5 we report the averages and rms scatters for  $\alpha$ -elements from the present and other studies: Minelli et al. (2021a); Wallerstein et al. (2007), who studied eight cool giants in NGC 6388 (we report the values from their analysis with photometric gravities); and the mean values from APOGEE DR17. As a further comparison, we added the average values derived from UVES and GIRAFFE spectra by Gratton et al. (2006, 2007, respectively) in NGC 6441, often considered a twin GC of NGC 6388, with similar origin and characteristics. Finally, the last two columns provide the values for NGC 6388 derived by M20, both from all available stars and by selecting stars with high S/Ns according to their criteria.

The values of  $[\text{Mg}/\text{Fe}]$  and  $[\text{Si}/\text{Fe}]$  from APOGEE DR17 are lower than those of the analyses based on optical spectra. They are also lower than the values given by M20, in particular when only high-S/N stars are used in their reanalysis with BACCHUS of an earlier SDSS/APOGEE release. On the contrary, the Ca level seems to be actually low in these GCs, with the notable exception of NGC 6441 from GIRAFFE spectra (see, however, the warning in Carretta and Bragaglia 2021, 2022b about the time on targets for NGC 6441 and the relative low S/N in that cluster).

In Fig. 11, we also compare the average abundances of Mg, Si, Ca, and Ti from the present work with the abundances in the GCs homogeneously analysed in our FLAMES survey (see Carretta et al. 2006 and following studies, referenced in Table B.1), represented by blue filled circles with error bars. These data have been complemented by four metal-rich GCs (three bulge clusters and one disc cluster) from Muñoz and collaborators. As reference, in the same figure we also plot field stars of the Galaxy, both in the halo and disc components (open grey circles) and in the bulge (cyan open circles), from several literature studies.

For the sake of clarity, all references to the data used are provided in Appendix B (Tables B.1 and B.2), where we also give the identification of each GC and its  $[\text{Fe}/\text{H}]$  value. Finally, we also plot abundances for the two more massive dwarf spheroidal galaxies associated with the MW, one still distinct (Fornax: Letarte et al. 2010, Lemasle et al. 2014) and the other already accreted and disrupting in the MW (Sagittarius, Minelli et al. 2021b). These stars are used as a robust benchmark for the pattern of  $\alpha$ -elements in external systems of lower total mass than the Galaxy. The combination of lower star formation and chemical evolution shows up in a lower metallicity knee and resulting underabundance of these elements, once such systems

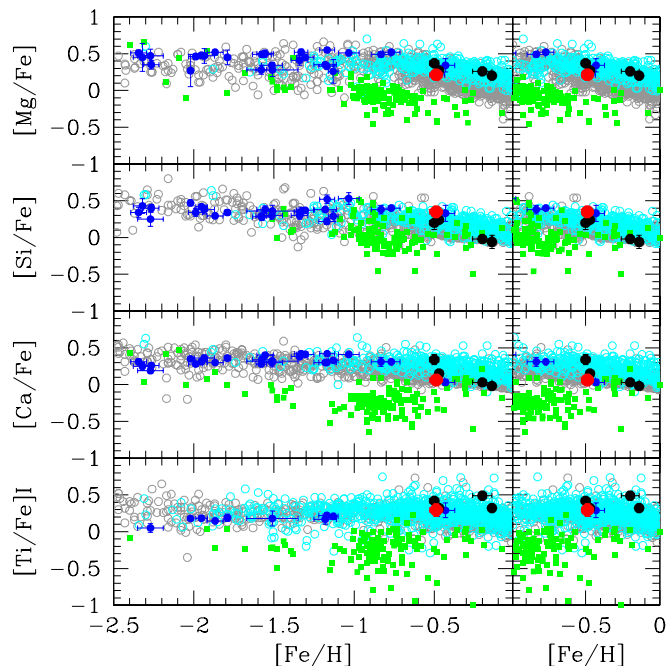


**Fig. 11.** Comparison of abundances of  $\alpha$ -elements with literature data. Left panels: Mean abundance ratios  $[\text{Mg}/\text{Fe}]$ ,  $[\text{Si}/\text{Fe}]$ ,  $[\text{Ca}/\text{Fe}]$ , and  $[\text{Ti}/\text{Fe}]$  (from top to bottom) as a function of metallicity from the homogeneous analysis of GCs in our FLAMES survey (filled blue points). Black filled circles are the average ratios in four metal-rich GCs from Muñoz and collaborators. The larger red point indicates NGC 6388 (present work). Grey and cyan open circles are field stars in the disc and bulge of the Milky Way, respectively, from different studies. References for all the data used in this figure are reported in Appendix B, Tables B.1 and B.2. Green filled squares are field stars in the dSph galaxies Fornax (Letarte et al. 2010, Lemasle et al. 2014) and Sagittarius (Minelli et al. 2021b). Right panels: Enlargement around the metallicity of NGC 6388.

were possibly accreted into the main Galaxy, as is currently happening to Sgr.

The average abundance of GCs nicely follows the pattern of  $\alpha$ -elements of field MW stars, a plateau at low metallicity followed by a decrease when the metallicity increases after the ‘knee’, signalling the major onset of SN Ia. As other metal-rich GCs ( $[\text{Fe}/\text{H}] \gtrsim -0.7$  dex), NGC 6388 participates in this trend well. In particular, the average  $[\text{Si}/\text{Fe}]$  ratios in NGC 6388 and in NGC 6441 are in very good agreement with the mean level shown by halo and disc GCs in the MW and with the abundance of bulge field stars, both giants (as in GCs) and dwarfs, as shown in detail in Fig. 12, where we display some of the studies used in Fig. 11, in a restricted range around the mean metallicity of NGC 6388.

Calcium abundances in NGC 6388 seem to lie at the lower envelope of the field bulge star distribution (Fig. 11). Overall, NGC 6388 and NGC 6441, together with the other bulge GCs (with the exception of NGC 6440, Muñoz et al. 2017) seem to be more compatible with the disc stars. However, the mean ratio  $[\text{Ca}/\text{Fe}]$  in NGC 6388 is still consistent with several studies focusing on bulge stars (Fig. 13), again taking into account small offsets related to the abundance analysis. Furthermore, we remind the reader that in NGC 6388, Ca is not involved into the network of proton-capture reactions (Carretta and Bragaglia 2021). This result is quantified in Fig. 7 and Table 4; among all relations concerning proton-capture elements, the only ones re-



**Table 5.** Averages and rms scatters for  $\alpha$ -element ratios in NGC 6388 and NGC 6441.

abund. ratio	this work UVES	this work GIRAFFE	M21	WKA07	APOGEE DR17	NGC 6441 G06	NGC 6441 G07	M20 all	M20 S/N>7
[Mg/Fe]	+0.212 0.049	+0.221 0.052		+0.259 0.175	+0.059 0.056	+0.34 0.09	+0.38 0.14	+0.069 0.167	+0.152 0.167
[Si/Fe]	+0.350 0.063	+0.309 0.061	+0.240 0.100	+0.368 0.158	+0.045 0.061	+0.33 0.11	+0.41 0.19	+0.118 0.190	+0.223 0.190
[Ca/Fe]	+0.062 0.049	+0.069 0.046	-0.018 0.071	-0.185 0.223	+0.032 0.074	+0.03 0.04	+0.21 0.19	+0.070 0.193	+0.130 0.193
[Ti/Fe] <sub>I</sub>	+0.295 0.086	+0.270 0.098	+0.115 0.087	-0.106 0.120	+0.132 0.177	+0.29 0.10	+0.33 0.20		
[Ti/Fe] <sub>II</sub>	+0.244 0.086			+0.294 0.128	+0.304 0.221	+0.33 0.14			

M21: Minelli et al. (2021a).

WKA07: Wallerstein, Kovtyukh, Andrievsky (2007).

G06,G07: Gratton et al. (2006: UVES); Gratton et al. (2007: GIRAFFE).

M20: Mészáros et al. (2020).

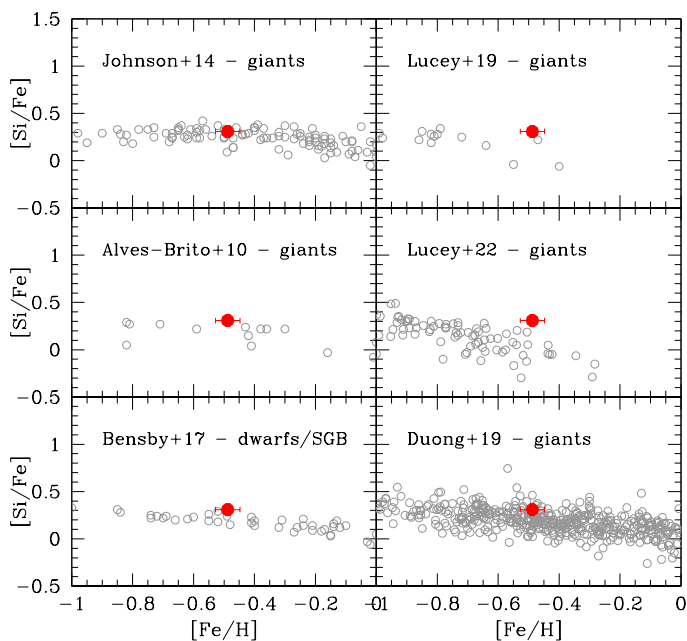


**Fig. 12.** Comparison of the average [Si/Fe] ratio in NGC 6388 (red point with error bar) to six different studies of bulge field stars in the metallicity range centred on the cluster: Johnson et al. (2014), Alves-Brito et al. (2010), Bensby et al. (2017), Lucey et al. (2019, 2022), and Duong et al. (2019). The evolutionary stage of each sample is reported in the panels.

sulting as statistically not significant are those involving Ca and Sc.

Among the species examined in Fig. 11, only Ti does not show the typical decline at high metallicity. We remark that this element is not a classical  $\alpha$ -element and is located at the boundary between  $\alpha$  and Fe-peak species. Moreover, Ti abundances are only available for less than a half of the GC sample, our FLAMES survey being focused on species (such as Mg, Si, and sometimes Ca) involved in the multiple population phenomenon. For the stars observed with UVES, both neutral and singly ionised lines were available. We found, on average, a difference of  $[\text{Ti}/\text{Fe}]_{\text{II}} - [\text{Ti}/\text{Fe}]_{\text{I}} = -0.051$  dex, with rms=0.096 dex, which is not significant.

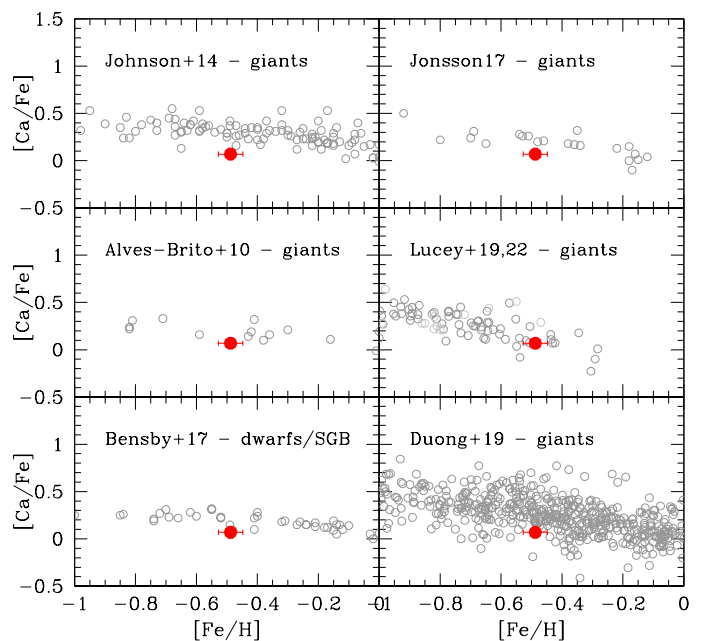


**Fig. 13.** Comparison of average [Ca/Fe] ratio in NGC 6388 (red point with error bar) to seven different studies of bulge field stars in the metallicity range centred on the cluster. To the studies listed in the previous figure, we added the work by Jönsson et al. (2017).

From this section, our results and the similarity between NGC 6388 and both the bulge and disc field of the MW suggest a high-mass environment for the progenitor of this cluster. Coupled with the chemo-dynamical evidence presented in a previous paper (CB22b), this is indicative of a formation within a massive component of the Galaxy, likely the bulge itself. The high metallicity of NGC 6388 clearly excludes this GC from being associated with a metal-poor structure recently reported from APOGEE data by Horta et al. (2021) and considered possibly accreted in the early MW before the presently observed main Galactic bulge (including its GC population and NGC 6388) was formed.

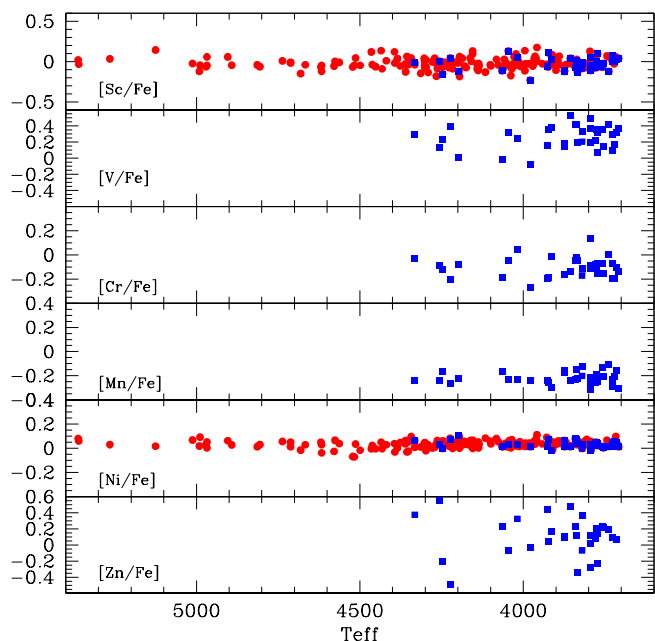


**Fig. 14.** Abundance ratios  $[\text{Sc}/\text{Fe}]_{\text{II}}$ ,  $[\text{V}/\text{Fe}]$ ,  $[\text{Cr}/\text{Fe}]_{\text{I}}$ ,  $[\text{Mn}/\text{Fe}]$ ,  $[\text{Ni}/\text{Fe}]$ , and  $[\text{Zn}/\text{Fe}]$  (from top to bottom) as a function of the effective temperature. Symbols are as in Fig. 10.

## 5.2. Fe-peak elements

Together with iron, we derived the abundances of seven species of the iron-peak group in NGC 6388:  $[\text{Sc}/\text{Fe}]_{\text{II}}$ ,  $[\text{V}/\text{Fe}]$ ,  $[\text{Cr}/\text{Fe}]_{\text{I}}$ ,  $[\text{Mn}/\text{Fe}]$ ,  $[\text{Ni}/\text{Fe}]$ ,  $[\text{Co}/\text{Fe}]$ , and  $[\text{Zn}/\text{Fe}]$ . Most abundances are derived from UVES spectra of the 12 stars newly observed in this work, integrated by the sample of Carretta and Bragaglia (2018). However, abundances of Sc and Ni are also measured for the larger sample of stars with GIRAFFE HR13 spectra, using on average 2 and 11 lines for Sc and Ni, respectively.

The derived abundances present no dependence on the temperature of stars over a range of about 1700 K (see Fig. 14), particularly evident in the cases of Sc and Ni, and are roughly clustered within  $\pm 0.10$  dex from the solar value, apart from V, which shows a slight overabundance, and Mn, which shows a clear deficiency, also reflected by the pattern of field stars at similar metallicity (see below).

In Carretta and Bragaglia (2022b) the average abundances of Sc, V, and Zn from the present work were used to check whether the level of these iron-peak elements could be used for chemically tagging NGC 6388 (accreted or formed in situ). Comparing the abundance of stars in NGC 6388 to a large ensemble of field stars (both disc and bulge stars) at similar metallicity, we were able to exclude a significant difference between cluster and field stars for all the three species under scrutiny, thus rejecting the accretion origin.

The in situ nature of NGC 6388 is supported and strengthened by the abundance of the other elements of the iron group derived here. In Fig. 15, we compare the mean abundances of Cr, Mn, Co, and Ni obtained for NGC 6388 to several samples of field stars in the Milky Way, together with the average abundances for a number of GCs from our FLAMES survey and from Muñoz and collaborators. No significant difference is found between cluster and field MW stars.

The same pattern is followed well by other classical, less massive bulge GCs, with the possible exception of Co, whose

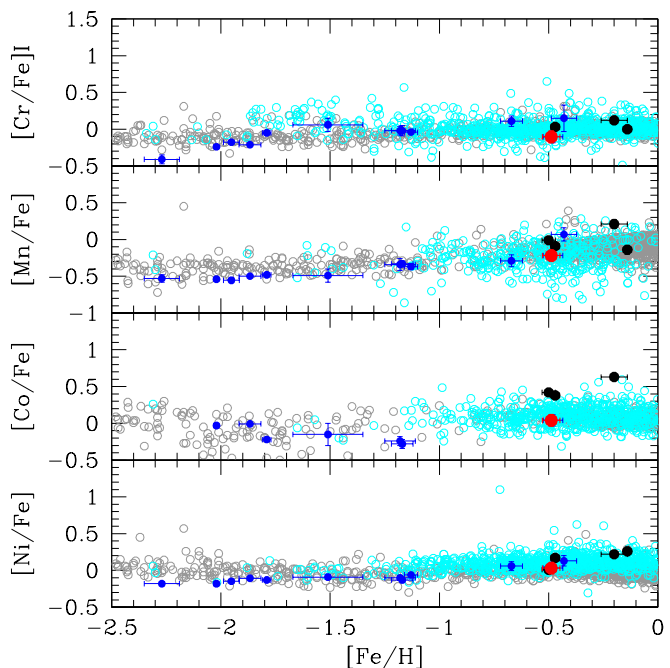


**Fig. 15.** Comparison of average abundance ratios  $[\text{Cr}/\text{Fe}]$ ,  $[\text{Mn}/\text{Fe}]$ ,  $[\text{Co}/\text{Fe}]$ , and  $[\text{Ni}/\text{Fe}]$  as a function of metallicity for NGC 6388, the GCs in our FLAMES survey, some metal-rich GCs from Muñoz and collaborators, and field stars in the disc and bulge of the Milky Way from several studies. Symbols are as in Fig. 11, and references are given in Appendix B.

level seems to exceed the locus defined by field bulge and disc stars. This is particularly evident for NGC 6528 (Muñoz et al. 2018). However, when NGC 6441 (Gratton et al. 2006) is also considered among the bulge populations, we may stress again that in general the iron-peak elements perform poorly, in picking up objects presumably of accreted origin.

## 5.3. Neutron-capture elements: Zr and Ba

We obtained the abundances of the neutron-capture elements Y, Zr, Ba, La, Ce, and Nd, sampling the first and second peak of species produced mainly by the *s*-process. We also measured Eu, typically produced by the *r*-process in the presence of higher neutron densities. Most abundances were obtained from UVES spectra, due to their larger spectral coverage. However, we were also able to derive Ba and Zr abundances from GIRAFFE HR13 spectra by measuring the Ba II 6141 Å line in all of the 150 stars and up to a maximum of five Zr I lines in 138 stars. We first concentrate on these two elements and defer the analysis of all others to the next sub-section.

Sources of atomic parameters for these Ba and Zr lines can be found in Table 8 of Gratton et al. (2007), with the exception of the  $\log g f$  value for the Ba II line, taken instead from Sneden et al. (2003). Due to the strength of this line and the consequent dependence on microturbulent velocity, abundances of Ba were derived using the relation as a function of surface gravity for  $v_t$  (Worley et al. 2013) and a constant metallicity value ( $-0.48$  dex) for all stars. This expedient allows us to avoid spurious trend of abundances as a function of the microturbulent velocity (see e.g. Carretta et al. 2015). The absence of trends with effective temperature for all derived elements is shown in Fig. 16.



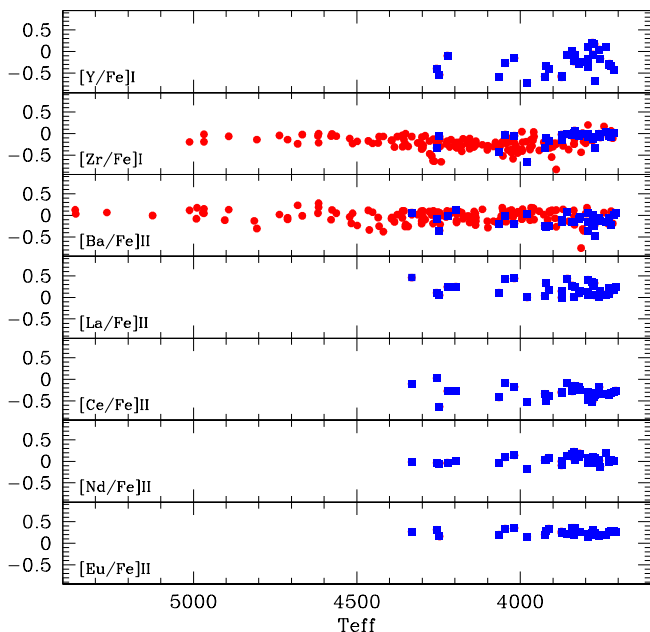


**Fig. 16.** Abundance ratios of neutron-capture elements in NGC 6388 as a function of the effective temperature. Red filled circles indicate stars with GIRAFFE spectra, whereas stars with UVES spectra are represented by blue filled squares.

Large samples of stars with abundances of *s*-process elements are necessary to explore another defining property of the type II GCs. Together with an enhancement in metallicity  $[\text{Fe}/\text{H}]$ , the metal-rich component is also proposed to be enriched in neutron-capture elements. This characteristic may manifest in a range of variations, going from the small amounts observed in NGC 1851 (Carretta et al. 2011) up to the large excesses detected in  $\omega$  Cen (Johnson and Pilachowski 2010; Marino et al. 2011b).

In Carretta and Bragaglia (2022a), we demonstrated that NGC 6388 is a typical mono-metallic GC, whose intrinsic spread in  $[\text{Fe}/\text{H}]$  is fully compatible with uncertainties derived from abundance analysis. Hence, finding here that neither Ba (measured in 185 stars) nor Zr (in 168 stars) show evidence of enhancement in part of the stars of this GC does not come as a surprise.

As a first test, we split our dataset at  $[\text{Fe}/\text{H}] = -0.488$  dex (the mean metallicity of the GIRAFFE sample). Then, we compared the cumulative distribution of Ba (and Zr) abundances for all stars more metal rich and more metal poor than this value using a Kolmogorov-Smirnov test. For both elements we obtain a K-S probability  $p \sim 0.30$ . This means that it is statistically not possible to safely reject the null hypothesis that the two distributions are extracted from the same parent population. A second test involves the pseudo-colour maps constructed using HST photometry (Milone et al. 2017). Figure 17 shows the chromosome map derived by us using the public data available from the HST archive (Nardiello et al. 2018; see Carretta and Bragaglia 2022a for details). In the figure, the stars in our sample falling in the small central region covered by the HST are indicated by larger symbols, coloured according to the derived Ba (upper panel) and Zr I (lower panel) abundances derived in the present work. There is no significant difference between stars scattered to the red in the pseudo-colour map and the other stars in this photometric plane. The direct implication of these tests is that NGC 6388

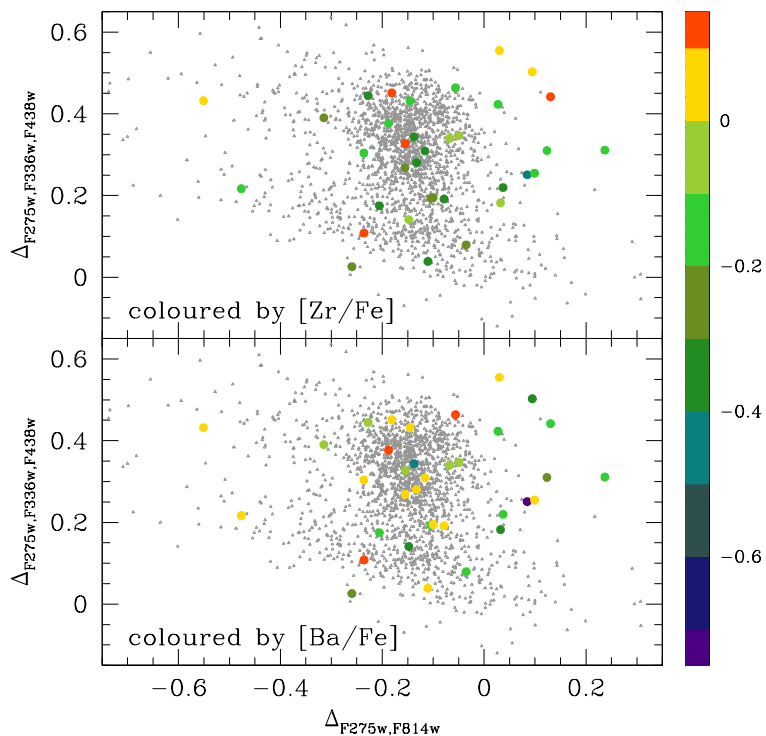


**Fig. 17.** Pseudo-colour maps of NGC 6388 from Carretta and Bragaglia (2022a). Larger symbols indicate stars of the present work cross-identified with the HST photometry in Nardiello et al. (2018). The colour-coding in the upper and bottom panels is done according to the abundances of Zr I and Ba, respectively, obtained in the present work.

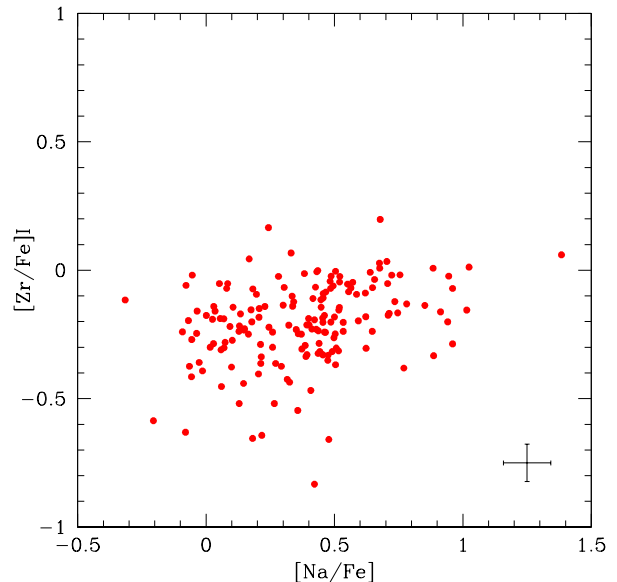


**Fig. 18.** Abundance ratio  $[\text{Zr}/\text{Fe}]_I$  as a function of  $[\text{Na}/\text{Fe}]$  in 168 stars of NGC 6388.

does not qualify as a type II GC either for some enhancement in metallicity or in the amount of *s*-process elements. In turn, the red RGB stars scattered in the pseudo-colour maps obtained from HST photometry are simply not yet explained by any observable change or alterations in their chemical composition.

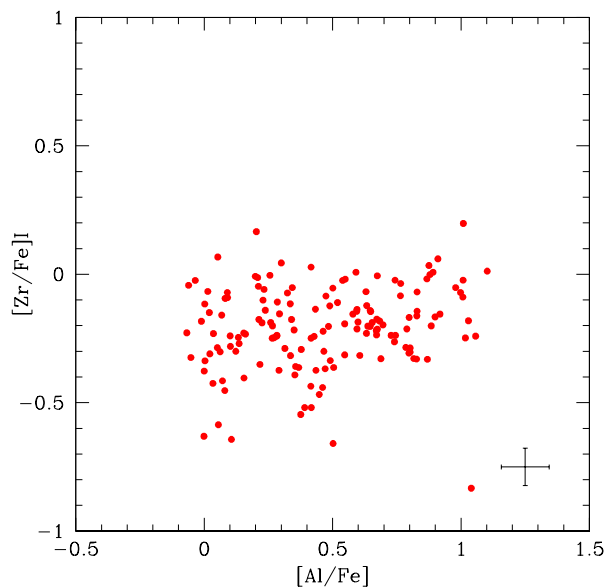


**Fig. 19.** As in Fig. 18, but for 151 stars with both Zr and Al abundances.

On the other hand, we found statistically significant correlations between the Zr abundance and a few light elements that are enhanced in the proton-capture reactions typical of the FG polluters. In Fig. 18 and Fig. 19, we show the ratio  $[Zr/Fe]_I$  as a function of  $[Na/Fe]$  and  $[Al/Fe]$ . We tested the level of significance for a linear regression between Zr and both Na and Al: the two-tail probabilities ( $p = 2.4 \times 10^{-5}$  and  $p = 0.033$  for Na and Al, respectively) allow us to conclude that the observed relations are real, with a high level of significance.

This is not the first time a similar correlation has been found. To our knowledge, the first paper to discuss correlations between elements enhanced in SG stars (such as Na) and others based on a large enough number of stars was Yong et al. (2013) on NGC 6752. They used differential analysis to derive very precise abundances (at 0.01 dex level) and found positive correlations, generally statistically significant, between many elements and Na. This could indicate that the same stars that enhanced Na over primordial values were also responsible for the increase in the other elements, among them some neutron-capture ones (unfortunately, they did not measure Zr). Their conclusion was that the abundance trends are real and discussed three potential mechanisms to explain them (besides the possibility of systematic errors in stellar parameters, which were regarded very unlikely): a star-to-star variation in CNO abundance, or in He (which is strictly connected to Na in multiple populations), or inhomogeneous early chemical evolution (i.e. metallicity variations). They favoured a combination of the last two, but encouraged similar studies on other clusters to try and clarify this issue.

At odds with those findings, Schiappacasse-Ulloa & Lucatello (2023) did not find correlation between Na and neutron-capture elements in the same cluster. They analysed about 160 stars in NGC 6752, from the main-sequence turn-off up to the RGB bump, deriving abundances of elements from different nucleosynthetic chains, among which we find Na, Y, and Ba. While they saw a mild Na-Y correlation, this is not statistically significant. Also, the Ba abundance does not correlate with Na abundance, and they concluded that the stars that enhanced the Na level did not contribute Y and Ba.

Finally, Kolomicas et al. (2022) derived the Na and Zr abundances of about 240 RGB stars in 47 Tuc, finding a statistically

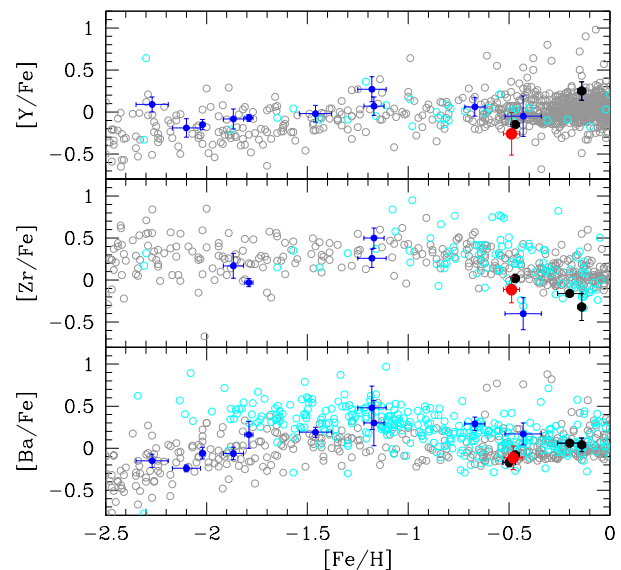


**Fig. 20.** As in Fig. 11, but for average abundance ratios  $[Y/Fe]$ ,  $[Zr/Fe]$ , and  $[Ba/Fe]$ . References for the samples are in Appendix B.

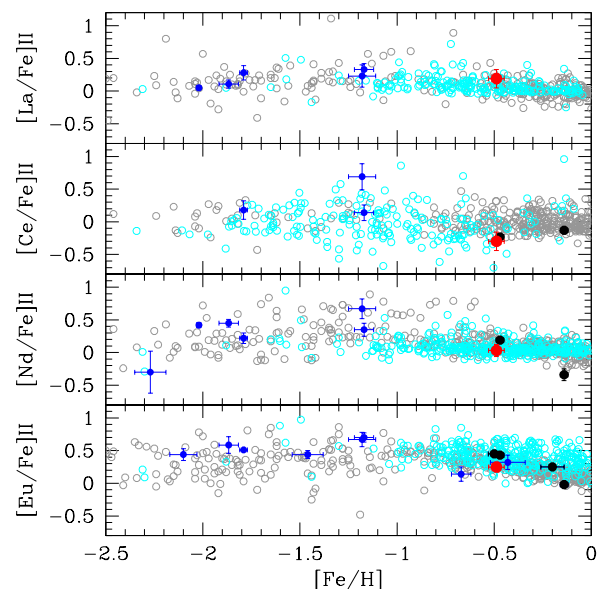


**Fig. 21.** As in Fig. 11, but for average abundance ratios  $[La/Fe]_{II}$ ,  $[Ce/Fe]_{II}$ ,  $[Nd/Fe]_{II}$ , and  $[Eu/Fe]_{II}$ . References for the samples are in Appendix B.

significant positive correlation between them. Their conclusion was that some amount of Zr should have been produced by the same primordial stars which were enriched in Na the SG stars. Unfortunately, this cannot be attributed unequivocally to a single class of polluters, either AGBs or massive stars, or a combination of the two. We follow Yong et al. (2013) and Kolomicas et al. (2022) in encouraging the extension of this kind of analysis to more elements and more clusters.

#### 5.4. Neutron-capture elements: Overall pattern in NGC 6388

The average abundances in NGC 6388 are compared to those of field disc and bulge stars, as well as to the mean abundances of previous analyses of GCs, in Fig. 20 and Fig. 21 (symbols

are as in Fig. 11). The neutron-capture elements in NGC 6388 seem to be consistent with those of bulge field stars of similar metallicity. Some offsets seem to exist with respect to the disc component around  $[\text{Fe}/\text{H}] \sim -0.5$  dex, but not enough to be very significant, maybe with the exception of Zr. However, the deficiency in  $[\text{Zr}/\text{Fe}]$  (middle panel of Fig. 20) is also shared by NGC 6441 and two other more metal-rich GCs. Together with the mean abundances of the four metal-poor GCs, the overall pattern could be explained by the decreasing abundances of Zr (produced in the main *s*-process component in AGB stars) as the metallicity increases due to the continuous injection of fresh iron from SN Ia (e.g. Tinsley 1979).

Another possibility is the one highlighted by Kobayashi et al. (2020); the contribution from nucleosynthetic sources with an intrinsically long time delay is more affected by the star formation timescale. Inefficient star formation (as in the halo) may give a higher level of neutron-capture elements relatively to iron. On the other hand, rapid star formation implies a smaller contribution of ejecta from longer lived, lower mass AGB stars, which are producers of elements from the main *s*-process component. However, this second alternative would apply to both the light and heavy *s*-process elements (Zr, La, Ce) produced in the main *s*-process, whereas there is some evidence that NGC 6388 and other bulge GCs show the same level of neutron-capture elements as seen in halo metal-poor GCs, at least for La, Ba, and Nd.

Concerning the *r*-process, in the bottom panel of Fig. 21 we trace the run of  $[\text{Eu}/\text{Fe}]$  as a function of metallicity. The pattern of constant values in the halo phase, followed by a gradual decrease as  $[\text{Fe}/\text{H}]$  increases, is explained well by the scenario pioneered by Tinsley (1979), pointing to the origin of Eu in the same sites (massive stars) where the  $\alpha$ -elements are produced. After the knee in  $[\text{Fe}/\text{H}]$  is reached in the main progenitor galaxy, the Eu production would remain essentially flat, but the  $[\text{Eu}/\text{Fe}]$  ratio is lowered by the increasing contribution of SN Ia. When our sample of clusters, mainly constituted by metal-poor GCs, is complemented by metal-rich GCs, it is easy to appreciate that the above scenario is satisfied by both field and GC stars. The interplay between enrichment from core-collapse and thermonuclear SNe was essentially the same, regardless of the star formation occurring in GCs or in the general field.

Finally, in Fig. 22 we use the relative strengths of the *r*-process and *s*-process to probe the relative contribution from high-mass stars (mainly responsible for yields of the weak component of the *s*-process and the *r*-process) and from low- or intermediate-mass AGB stars (main *s*-process). In this figure, the pure *r*-process element Eu is compared to Y, chosen as reference element for the *s*-process. Again, by plotting the ratio  $[\text{Eu}/\text{Y}]$  as a function of the metallicity (liberally used as a chemical ‘chronometer’) we are exploiting the different mass ranges, and therefore different evolutionary timescales, of the involved stars to give a general picture of the enrichment process in field and GC stars.

At low metallicities, both GC and field stars show high  $[\text{Eu}/\text{Y}]$  ratios, approaching the scaled Solar System pure *r*-process level, with scarce or no contribution from the *s*-process in AGB stars. As lower mass stars with longer evolutionary timescales appear on the enrichment scene, an increase in the production of *s*-process elements lowers the  $[\text{Eu}/\text{Y}]$  ratio. The decrease seems to happen in lockstep both in field and GC stars until about  $[\text{Fe}/\text{H}] \sim -0.5$ . At this metallicity, our present analysis does confirm the earlier results presented in Carretta et al. (2007a) for NGC 6388 and in Gratton et al. (2006) for NGC 6441. In particular, NGC 6388 seems to have a  $[\text{Eu}/\text{Y}]$

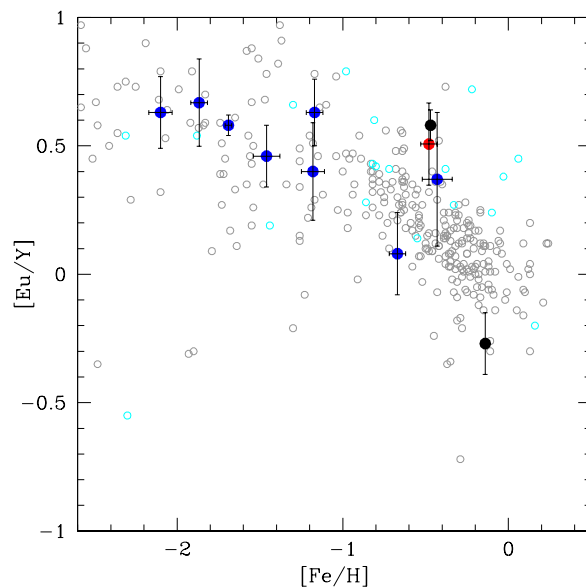


**Fig. 22.** As in Fig. 11, but for the average abundance ratio  $[\text{Eu}/\text{Y}]$  of the Eu and Y species, which are reference elements for the *r* and *s*-processes, respectively. Field bulge stars (cyan) are from Lucey et al. (2019) and Gratton et al. (2006). Halo and disc stars (grey circles) are from James et al. (2004) and the compilation by Venn et al. (2004).

higher than observed in field stars of similar metallicities. Although the larger errors associated with NGC 6441 make its ratio still compatible with the field stars, the ratio in NGC 6388 is in better agreement with the ratio in metal-poor GCs, where the contribution of AGB stars to the *s*-process was not yet relevant.

In Carretta et al. (2007a), we put forward the hypothesis that this excess in  $[\text{Eu}/\text{Y}]$  could be explained by an enhanced contribution of massive stars to the enrichment in the bulge, since light *s*-process elements such as Y can be also produced in the weak *s*-process component within the He-burning core of massive stars (Couch et al. 1974, Travaglio et al. 2004). This idea would also explain the high  $[\text{Eu}/\text{Y}]$  ratios measured in metal-rich bulge field stars (Gratton et al. 2006, cyan circles in Fig. 22). However, we note that the disc GC NGC 5927 (Mura-Guzmán et al. 2018) also shares this excess ratio; therefore, a larger sample of GCs at high metallicity is required to answer the question.

A more quantitative approach is summarised in Fig. 23, where we compare the average abundances of neutron-capture elements derived from UVES spectra in NGC 6388 to the ratios of *r*- and *s*-elements estimated by Simmerer et al. (2004) in the Solar System. For this comparison we followed the approach suggested by Raffaele Gratton and employed in Carretta et al. (2015) for NGC 6093. To reproduce the pattern of neutron-capture elements in NGC 6388, our best fit must consider the sum of two contributions: a solar-scaled *r*-process contribution, with a scaling by  $-0.27$  dex, and a solar-scaled *s*-process contribution, with a scaling by  $-0.51$  dex. Taking into account the derived metallicity for NGC 6388 ( $[\text{Fe}/\text{H}] = -0.48$  dex), these scaling factors imply abundance ratios of  $[r/\text{Fe}] = +0.21$  dex and  $[s/\text{Fe}] = -0.03$  dex.

The excess of elements produced by the *r*-process is very similar to the one we obtain from the  $\alpha$ -elements. From GIRAFFE and UVES spectra, we derive mean values of  $[\alpha/\text{Fe}] = +0.22$  dex and  $+0.23$  dex (regardless of inclusion or exclusion of Mg in the average). The excess in *r*-process elements with respect to the solar value may be interpreted as an iron deficiency

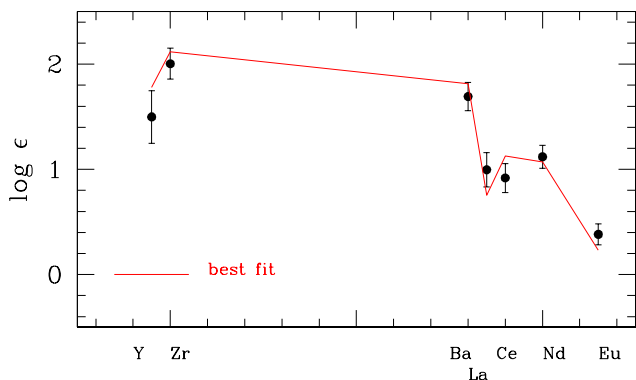


**Fig. 23.** Average abundances of Y, Zr, Ba, La, Ce, Nd, and Eu in NGC 6388 from UVES spectra. The respective rms scatters are also represented as associated error bars. Our best-fit estimate using solar-scaled pure  $r$ -process and  $s$ -process abundances is shown as a red line (see text for the adopted procedure).

due to the fact that we see almost exclusively the contribution of massive stars, whereas the one from SN Ia is missing. On the other side, our data show that it is necessary to also consider a significant part of the  $s$ -process, which scale almost exactly as Fe, to explain the observations in NGC 6388 well.

## 6. Summary and conclusions

We present the homogeneous spectroscopic analysis of a large sample of stars in NGC 6388. Concerning the proton-capture elements, we find that all stars observed in NGC 6388 nicely trace the typical correlations and anti-correlations that are the unique trademark of GCs. The exceptions are the heaviest species (Ca, Sc) involved in the network of proton-capture reactions in H-burning at high temperature. No statistically significant variation is found for these two species between FG and SG stars, confirming qualitative results shown in Carretta and Bragaglia (2019) for NGC 6388.

Star-to-star variations in Si, correlated to abundance changes in Al and anti-correlated to Mg depletions, support leakage from the Mg-Al cycle on Si. In turn, this requires temperatures as high as about 65 MK in the FG polluters.

A simple dilution model is compatible with a single class of polluters injecting processed matter in the intra-cluster medium at early time in the proto-GC. Mixing this polluted material (typical of the composition of the SG group E) with different amounts of pristine gas (whose composition is represented by the P group of stars), we can obtain a good agreement for the composition of the intermediate SG group for all the involved species.

The extent of the Na-O anti-correlation, the privileged, unambiguous signature of multiple stellar populations in GCs, seems to be too short in NGC 6388 with respect to its large total mass. Together with a few other massive GCs (47 Tuc, M 15, NGC 6441), NGC 6388 lies slightly below the main trend in the IQR[O/Na] versus  $M_V$  relation describing the dependence of the extent of Na-O anti-correlation as a function of cluster total mass (Carretta 2006; Carretta et al. 2010a).

The inventory of  $\alpha$ -element abundances in NGC 6388 is very compatible with the chemical pattern of field stars in the Milky Way, both in the disc and bulge. The abundance ratios in NGC 6388 participate in the classical trend defined by the interplay between star formation and lifetimes of the main stellar

nucleosynthesis sites, namely type II and type Ia SNe. The resulting plateau at low metallicity, followed by a knee and the decrease of  $\alpha$ /Fe ratio at increasing [Fe/H] is followed by both field and GC stars, including NGC 6388.

We found no evidence of a low level of Si, as derived by infrared APOGEE data. Therefore, we cannot support an extragalactic origin for NGC 6388, as suggested by Horta et al. (2020). We note that all the studies using optical spectroscopy converge on finding normal, high values of [Si/Fe] for NGC 6388. It seems that there could be some offsets between optical and infrared analyses due to still poorly understood effects concerning Si. A low value of Ca is instead derived for NGC 6388, as well as for bulge stars in a similar metallicity regime, regardless of whether optical or infrared spectra are used.

The average abundances of elements of the iron group in NGC 6388 closely follow the pattern of chemical enrichment typical of field stars in the Milky Way. We then confirm and strengthen the results by Carretta and Bragaglia (2022b): NGC 6388 is clearly not of extragalactic origin, but likely formed in situ in the Galactic bulge, and the iron-peak species can only be used to trace the GCs of the Sagittarius dwarf, whose content in such elements is typically lower than in the autochthonous stars of our Galaxy. Consistently, both these elements and the high Si level, normal for old GCs, point toward the in situ origin of NGC 6388.

We do not detect any signature of enhancement in neutron-capture elements in a fraction of stars of NGC 6388. In particular, there is no significant difference in the abundance of Ba and Zr between FGs, SG stars, and the stars scattered to the red of the RGB. This evidence corroborates the fact that NGC 6388 is not a GC of a distinct (type II) class and also leaves the red RGB stars unexplained, at least from a chemical perspective.

Statistically significant correlations are found between Zr abundance and both Na and Al abundances. Similar results are also found in a few other cases and warrant being extended to a larger sample of GCs.

The excess of the  $r$ -process element Eu in NGC 6388 is consistent with the values of more metal-poor old GCs and similar to the ratio of  $\alpha$ -elements, showing the contribution of massive stars coupled to the small injection of Fe from thermonuclear SNe at the epoch of cluster formation. The overall pattern of neutron-capture elements from high-resolution UVES spectra shows, however, that it is necessary to also consider a contribution from the  $s$ -process in this GC.

*Acknowledgements.* This research made use of the products of the Cosmic-Lab project funded by the European Research Council. We thank E. Dalessandro for helpful discussions. This research has made use of the SIMBAD database (in particular VizieR), operated at CDS, Strasbourg, France, of the NASA's Astrophysical Data System, and of TOPCAT (<http://www.starlink.ac.uk/topcat/>). This paper makes use of the data collected by the HST Treasury Program GO 13297. We acknowledge funding from PRIN INAF 2019 "Building up the halo: chemo-dynamical tagging in the age of large surveys", PI Lucatello.

## References

- Abdurro'uf, Accetta, K., Aerts, C., et al. 2022, ApJS, 259, 35
- Adibekyan, V.Zh., Sousa, S.G., Santos, N.C. et al. 2012, A&A, 545, A32
- Alonso, A., Arribas, S., Martínez-Roger, C. 1999, A&AS, 140, 261
- Alonso, A., Arribas, S., Martínez-Roger, C. 2001, A&A, 376, 1039
- Alves-Brito, A., Meléndez, J., Asplund, M., Ramirez, I., Yong, D. 2010, A&A, 513, A35
- Anders, E., Grevesse, N. 1989, GeCoA, 53, 197
- Arnould, M., Goriely, S., Jorissen, A. 1999, A&A, 347, 572
- Barbuy, B., Hill, V., Zoccali, M. et al. 2013, A&A, 559, A5
- Bastian, N., Lardo, C. 2018, ARA&A, 56, 83



- Battistini, C., Bensby, T. 2016, *A&A*, 586, A49
- Beirão, P., Santos, N.C., Israelian, G., Mayor, M. 2005, *A&A*, 438, 251
- Bensby, T., Feltzing, S., Lundström, I., Ilyin, I. 2005, *A&A*, 433, 185
- Bensby, T., Feltzing, S., Oey, M.S. 2014, *A&A*, 562, A71
- Bensby, T., Feltzing, S., Gould, A. et al. 2017, *A&A*, 605, A89
- Böhm-Vitense, E. 1979, *ApJ*, 234, 521
- Bragaglia, A., Carretta, E., Gratton, R.G. et al. 2001, *AJ*, 121, 327
- Bragaglia, A., Carretta, E., D’Orazi, V. et al. 2017, *A&A*, 607, A44
- Brewer, J.M., Fischer, D.A., Valenti, J.A., Piskunov, N. 2016, *ApJS*, 225, 32
- Carretta, E. 2006, *AJ*, 131, 1766
- Carretta, E. 2015, *ApJ*, 810, 148
- Carretta, E., Bragaglia, A. 2018, *A&A*, 614, A109
- Carretta, E., Bragaglia, A. 2019, *A&A*, 627, L7
- Carretta, E., Bragaglia, A. 2021, *A&A*, 646, A9
- Carretta, E., Bragaglia, A. 2022a, *A&A*, 659, A122
- Carretta, E., Bragaglia, A. 2022b, *A&A*, 660, L1
- Carretta, E., Gratton R.G., Bragaglia, A., Bonifacio, P., Pasquini, L. 2004, *A&A*, 416, 925
- Carretta, E., Bragaglia, A., Gratton, R.G. et al. 2006, *A&A*, 450, 523
- Carretta, E., Bragaglia, A., Gratton, R.G. et al. 2007a, *A&A*, 464, 967
- Carretta, E., Recio-Blanco, A., Gratton, R.G., Piotto, G., Bragaglia, A. 2007b, *ApJ*, 671, L125
- Carretta, E., Bragaglia, A., Gratton, R.G., Lucatello, S. 2009a, *A&A*, 505, 139
- Carretta, E., Bragaglia, A., Gratton, R.G. et al. 2009b, *A&A*, 505, 117
- Carretta, E., Bragaglia, A., Gratton, R.G., D’Orazi, V., Lucatello, S. 2009c, *A&A*, 508, 695
- Carretta, E., Bragaglia, A., Gratton, R.G. et al. 2010a, *A&A*, 516, 55
- Carretta, E., Bragaglia, A., Gratton, R.G. et al. 2010b, *ApJ*, 712, L21
- Carretta, E., Bragaglia, A., Gratton, R.G. et al. 2010c, *A&A*, 520, 95
- Carretta, E., Lucatello, S., Gratton, R.G., Bragaglia, A., D’Orazi, V. 2011, *A&A*, 533, 69
- Carretta, E., Bragaglia, A., Gratton, R.G., Lucatello, S., D’Orazi, V. 2012, *ApJ*, 750, L14
- Carretta, E., Bragaglia, A., Gratton, R.G. et al. 2013, *A&A*, 557, A138
- Carretta, E., Bragaglia, A., Gratton, R.G. et al. 2014a, *A&A*, 561, A87
- Carretta, E., Bragaglia, A., Gratton, R.G. et al. 2014b, *A&A*, 564, A60
- Carretta, E., Bragaglia, A., Gratton, R.G. et al. 2015, *A&A*, 578, A116
- Carretta, E., Bragaglia, A., Lucatello, S. et al. 2017, *A&A*, 600, A118
- Chen, J., Ferraro, F.R., Cadelano, M., et al. 2021, *Nature Astronomy*, 5, 1170
- Cohen, J.G., Kirby, E.N. 2012, *ApJ*, 760, 86
- Couch, R.G., Schmiedekamp, A.B., Arnett, W.D. 1974, *ApJ*, 190, 95
- Cordero, M.J., Pilachowski, C.A., Johnson C.I. et al. 2014, *ApJ*, 780, 94
- D’Antona, F., Caloi, V., Montalbán, J., Ventura, P., Gratton, R. 2002, *A&A*, 395, 69
- D’Antona, F., Vesperini, E., D’Ercole, A. et al. 2016, *MNRAS*, 458, 2122
- da Silveira, C.R., Barbuy, B., Friaça, A.C.S. et al. 2018, *A&A*, 614, A149
- Delgado Mena, E., Tsantaki, M., Adibekyan, V. Zh. et al. 2017, *A&A*, 606, A94
- Duong, L., Asplund, M., Nataf, D.M. et al. 2019, *MNRAS*, 486, 3586
- Duong, L., Asplund, M., Nataf, D.M., Freeman, K.C., Ness, M. 2019, *MNRAS*, 486, 5349
- Ferraro, F.R., Carretta, E., Corsi, C. E., et al. 1997, *A&A*, 320, 757
- Forsberg, R., Jönsson, H., Ryde, N., Mattucci, F. 2019, *A&A*, 631, A113
- Gratton, R.G. 1988, *Rome Obs. Preprint Ser.*, 29
- Gratton, R.G., Carretta, E., Eriksson, K., Gustafsson, B. 1999, *A&A*, 350, 955
- Gratton, R.G., Bonifacio, P., Bragaglia, A., et al. 2001, *A&A*, 369, 87
- Gratton, R.G., Carretta, E., Claudi, R., Lucatello, S., Barbieri, M. 2003, *A&A*, 404, 187
- Gratton, R.G., Snenen, C., Carretta, E. 2004, *ARA&A*, 42, 385
- Gratton, R.G., Lucatello, S., Bragaglia, A. et al. 2006, *A&A*, 455, 271
- Gratton, R.G., Lucatello, S., Bragaglia, A. et al. 2007, *A&A*, 464, 953
- Gratton, R.G., Lucatello, S., Carretta, E. et al. 2011, *A&A*, 534, 123
- Gratton, R.G., Carretta, E., Bragaglia, A. 2012a, *A&ARv*, 20, 50
- Gratton, R.G., Lucatello, S., Carretta, E. et al. 2012b, *A&A*, 539, 19
- Gratton, R.G., Lucatello, S., Sollima, A. et al. 2013, *A&A*, 549, A41
- Gratton, R.G., Lucatello, S., Sollima, A. et al. 2014, 563, A13
- Gratton, R.G., Lucatello, S., Sollima, A. et al. 2015, *A&A*, 573, A92
- Gratton, R.G., Bragaglia, A., Carretta, E. et al. 2019, *A&ARv*, 27, 8
- Harris, W. E. 2010, arXiv:1012.3224
- Horta, D., Schiavon, R.P., Mackereth, J.T. et al. 2020, *MNRAS*, 493, 3363
- Horta, D., Schiavon, R.P., Mackereth, J.T. et al. 2021, *MNRAS*, 500, 1385
- Ishigaki, M.N., Chiba, M., Aoki, W. 2012, *ApJ*, 753, 64
- Ishigaki, M.N., Aoki, W., Chiba, M. 2013, *ApJ*, 771, 67
- James, G., François, P., Bonifacio, P. et al. 2004a, *A&A*, 427, 825
- James, G., François, P., Bonifacio, P. et al. 2004b, *A&A*, 414, 1071
- Johnson, C.I., Pilachowski, C.A. 2010, *ApJ*, 722, 1373
- Johnson, C.I., Rich, R.M., Kobayashi, C., Kunder, A., Koch, A. et al. 2014, *AJ*, 148, 67
- Jönsson, H., Ryde, N., Schultheis, M., Zoccali, M. 2017, *A&A*, 598, A101
- Karakas, A.I., Lattanzio, J.C. 2003, *PASA*, 20, 279
- Kobayashi, C., Karakas, A.I., Lugaro, M. 2020, *ApJ*, 900, 179
- Kolomicas, E., Dobrovolskas, V., Kučinskas, A., Bonifacio, P., Korotin, S. 2022, *A&A*, 660, A46
- Kurucz, R.L. 1993, CD-ROM 13, Smithsonian Astrophysical Observatory, Cambridge
- Lai, D.K., Bolte, M., Johnson, J.A. et al. 2008, *ApJ*, 681, 1524
- Lanzoni, B., Mucciarelli, A., Origlia, L. et al. 2013, *ApJ*, 769, 107 (L13)
- Lemasle, B., de Boer, T.J.L., Hill, V. et al. 2014, *A&A*, 572, 88
- Letarte, B., Hill, V., Tolstoy, E. et al. 2010, *A&A*, 523, 17
- Lomaeva, M., Jönsson, H., Ryde, N., Schultheis, M., Thorsbro, B. 2019, *A&A*, 625, A141
- Lucey, M., Hawkins, K., Ness, M. et al. 2019, *MNRAS*, 488, 2283
- Lucey, M., Hawkins, K., Ness, M. et al. 2022, *MNRAS*, 509, 122
- Magain, P. 1984, *A&A*, 134, 189
- Marino, A.F., Milone, A., Piotto, G., et al. 2011b, *ApJ*, 731, 64
- Marino, A.F., Villanova, S., Milone, A.P. et al. 2011a, *ApJ*, 730, L16
- Massari, D., Koppelman, H.H., Helmi, A. 2019, *A&A*, 630, L4
- Mészáros, S., Masseron, T., García-Hernández, D.A. et al. 2020, *MNRAS*, 492, 1641 (M20)
- Milone, A.P., Marino, A.F., Renzini, A. et al. 2018, *MNRAS*, 481, 5098
- Minelli, A., Mucciarelli, A., Massari, D., et al. 2021a, *ApJL*, 918, L32
- Minelli, A., Mucciarelli, A., Romano, D., et al. 2021b, *ApJ*, 910, 114
- Mucciarelli, A., Bellazzini, M., Ibata, R. et al. 2012, *MNRAS*, 426, 2889
- Mucciarelli, A., Bellazzini, M., Merle, T. et al. 2015, *ApJ*, 801, 68
- Muñoz, C., Villanova, S., Geisler, D. et al. 2017, *A&A*, 605, A12
- Muñoz, C., Geisler, D., Villanova, S. et al. 2018, *A&A*, 620, A96
- Muñoz, C., Villanova, S., Geisler, D. et al. 2020, *MNRAS*, 492, 3742
- Mura-Guzmán, A., Villanova, S., Muñoz, C. 2018, *MNRAS*, 474, 4541
- Myeong, G.C., Vasiliev, E., Iorio, G. 2019, *MNRAS*, 488, 1235
- Nardiello, D., Libralato, M., Piotto, G. et al. 2018, *MNRAS*, 481, 3382
- Neves, V., Santos, N.C., Sousa, S.G., Correia, A.C.M., Israelian, G. 2009, *A&A*, 497, 563
- Prantzos, N., Charbonnel, C., Iliadis, C. 2017, *A&A*, 608, A28
- R Core Team (2022). R: A language and environment for statistical computing. R Foundation for Statistical Computing, Vienna, Austria. URL <https://www.R-project.org/>
- Reddy, B.E., Tomkin, J., Lambert, D.L., Allende Prieto, C. 2003, *MNRAS*, 340, 304
- Reddy, B.E., Lambert, D.L., Allende Prieto, C. 2006, *MNRAS*, 367, 1329
- Reggiani, H., Meléndez, J., Kobayashi, C., Karakas, A., Placco, V. 2017, *A&A*, 608, A46
- Roederer, I.U., Presto, G.W., Thompson, I.B. et al. 2014, *AJ*, 147, 136
- Schiappacasse-Ulloa, J., Lucatello, S. 2023, *MNRAS*, 520, 5938
- Simmerer, J., Snenen, C., Cowan, J.J. et al. 2004, *ApJ*, 617, 1091
- Smith, V.V., Bizyaev, D., Cunha, K. et al. 2021, *AJ*, 161, 254
- Snenen, C., Kraft, R.P., Shetrone, M.D. et al. 1997, *AJ*, 114, 1964
- Snenen, C., Cowan, J.J., Lawler, J.E. et al. 2003, *ApJ*, 591, 936
- Tinsley, B.M. 1979, *ApJ*, 229, 1046
- Tolstoy, E., Hill, V., Tosi, M. 2009, *ARA&A*, 47, 371g
- Travaglio, C., Gallino, R., Arnone, E. et al. 2004, *ApJ*, 601, 864
- Valle, G., Dell’Omodarme, M., Tognelli, E. 2022, *A&A*, 658, A141
- Vasiliev, E., Baumgardt, H. 2021, *MNRAS*, 505, 5978
- Ventura, P., D’Antona, F., Di Criscienzo, M. et al. 2012, *ApJ*, 761, L30
- Villanova, S., Piotto, G., Gratton, R.G. 2009, *A&A*, 499, 755
- Villanova, S., Geisler, D., Piotto, G., Gratton, R.G. 2012, *ApJ*, 748, 62
- Wallerstein, G., Kovtyukh, V.V., Andrievsky, S.M. 2007, *AJ*, 133, 1373
- Worley, C.C., Hill, V., Sobek, J., Carretta, E. 2013, *A&A*, 553, A47
- Yong, D., Grundahl, F., Nissen, P.E., Jensen, H.R., Lambert, D.L. 2005, *A&A*, 438, 875
- Yong, D., Meléndez, J., Grundahl, F. et al. 2013, *MNRAS*, 434, 3452

## Appendix A: Abundances of individual stars

Abundances for individual stars in NGC 6388 are listed in Table A.1 for proton-capture elements, Table A.2 for  $\alpha$ -elements, Table A.3 for elements of the Fe-group, and Table A.4 for species from neutron-capture processes measured on UVES spectra. Finally, in Table A.5 we list the abundances of the neutron-capture elements Zr I and Ba II that could be derived also from GIRAFFE spectra. For this table, as well as for tables relative to light elements,  $\alpha$ -elements and Fe-peak elements (Tables A.1, A.2, A.3, and A.5), only an excerpt is provided here as a guidance of the content. Complete tables can be found at CDS Strasbourg.



Table A.1. Light element abundances.

Star	nr	[O/Fe] <sub>I</sub>	rms	lim	nr	[Na/Fe] <sub>I</sub>	rms	nr	[Mg/Fe] <sub>I</sub>	rms	nr	[Al/Fe] <sub>I</sub>	rms	phase
n63a	2	-0.099	0.110	1	4	+0.215	0.066	4	+0.198	0.133	2	+0.003	0.031	RGB
n63b	2	-0.149	0.137	1	3	+0.111	0.041	3	+0.265	0.067	2	+0.265	0.027	RGB
n63c	2	-0.372	0.157	1	4	+0.884	0.090	4	+0.143	0.097	2	+0.891	0.151	RGB
n63d	2	-0.242	0.075	1	4	+0.497	0.060	4	+0.234	0.099	2	+0.091	0.083	RGB
n63e	2	-0.159	0.053	1	4	+0.551	0.050	4	+0.230	0.173	2	+0.501	0.071	RGB
n63f	2	-0.112	0.002	1	4	+0.639	0.085	4	+0.223	0.116	2	+0.199	0.126	RGB
n63g	1	-0.633		1	3	+1.267	0.120	4	+0.191	0.063	2	+1.218	0.088	RGB
n63h	2	-0.061	0.013	1	4	+0.196	0.044	4	+0.202	0.104	2	+0.081	0.071	RGB
n63i	2	-0.047	0.008	1	4	+0.586	0.179	4	+0.251	0.078	2	+0.083	0.018	RGB
n63l	2	+0.001	0.023	1	4	+0.207	0.126	4	+0.192	0.063	2	+0.020	0.108	RGB
n63m	2	-0.200	0.083	1	4	+0.735	0.112	4	+0.222	0.146	2	+0.633	0.159	RGB
n63n	2	-0.445	0.043	1	4	+0.648	0.085	4	+0.115	0.148	2	+0.630	0.163	RGB
l63p001	2	+0.237	0.001	1	2	+0.383	0.082	2	+0.259	0.031	2	+0.208	0.018	RGB
l63p002	2	+0.301	0.105	1	2	+0.229	0.001	2	+0.380	0.030	2	+0.646	0.218	RGB
l63p003	1	+0.021		0	2	+0.348	0.075	2	+0.323	0.035	1	+0.025		RGB
l63p004	2	+0.245	0.113	1	2	-0.315	0.142	2	+0.215	0.083	2	+0.002	0.080	RGB
l63p006	1	+0.120		1	2	+0.426	0.063	2	+0.246	0.104	0			RGB

Table A.2.  $\alpha$ -element abundances.

Star	nr	[Si/Fe] <sub>I</sub>	rms	nr	[Ca/Fe] <sub>I</sub>	rms	nr	[Ti/Fe] <sub>I</sub>	rms	nr	[Ti/Fe] <sub>II</sub>	rms
n63a	9	+0.358	0.166	16	+0.034	0.140	25	+0.171	0.211	11	+0.264	0.254
n63b	0			11	+0.040	0.225	25	+0.325	0.189	8	+0.357	0.201
n63c	8	+0.364	0.167	18	+0.098	0.222	29	+0.288	0.271	11	+0.274	0.143
n63d	6	+0.319	0.148	16	+0.087	0.206	28	+0.322	0.170	12	+0.246	0.163
n63e	8	+0.327	0.180	19	+0.072	0.177	26	+0.272	0.151	12	+0.307	0.194
n63f	8	+0.310	0.172	19	+0.152	0.198	27	+0.320	0.182	12	+0.303	0.174
n63g	8	+0.288	0.278	9	+0.081	0.217	21	+0.378	0.220	10	+0.324	0.230
n63h	9	+0.368	0.194	15	+0.026	0.114	27	+0.277	0.164	10	+0.205	0.236
n63i	8	+0.353	0.151	19	+0.052	0.164	27	+0.309	0.153	12	+0.263	0.149
n63l	8	+0.339	0.158	17	+0.051	0.149	28	+0.263	0.179	11	+0.292	0.176
n63m	7	+0.359	0.198	17	+0.121	0.174	27	+0.314	0.261	10	+0.265	0.176
n63n	9	+0.382	0.259	13	+0.172	0.202	27	+0.267	0.225	11	+0.288	0.289
l63p001	3	+0.262	0.060	6	+0.139	0.088	3	+0.298	0.074	0		
l63p002	3	+0.243	0.031	6	+0.028	0.112	3	+0.294	0.084	0		
l63p003	3	+0.166	0.006	6	+0.159	0.116	2	+0.288	0.098	0		
l63p004	3	+0.219	0.084	5	+0.101	0.054	3	+0.139	0.130	0		
l63p006	3	+0.270	0.062	6	+0.061	0.160	4	+0.256	0.172	0		

Table A.3. Iron-peak abundances.

Star	nr	[Sc/Fe] <sub>I</sub>	rms	nr	[V/Fe] <sub>I</sub>	rms	nr	[Cr/Fe] <sub>I</sub>	rms	nr	[Mn/Fe] <sub>I</sub>	rms	nr	[Co/Fe] <sub>I</sub>	rms	nr	[Ni/Fe] <sub>I</sub>	rms	nr	[Zn/Fe] <sub>I</sub>	rms
n63a	8	-0.035	0.134	13	+0.069	0.261	17	-0.155	0.230	8	-0.247	0.244	5	-0.027	0.283	41	+0.023	0.209	1	+0.137	
n63b	3	+0.072	0.239	8	+0.100	0.266	15	-0.066	0.211	8	-0.231	0.295	5	+0.083	0.334	26	+0.018	0.358	0		
n63c	8	+0.026	0.155	13	+0.321	0.236	21	-0.107	0.284	7	-0.153	0.095	5	+0.047	0.175	40	+0.045	0.280	1	+0.066	
n63d	7	+0.004	0.220	13	+0.167	0.246	17	-0.194	0.194	8	-0.204	0.182	5	+0.111	0.178	31	+0.054	0.171	0		
n63e	8	-0.086	0.125	11	+0.205	0.205	25	-0.170	0.253	6	-0.202	0.204	5	+0.077	0.143	43	-0.001	0.185	1	-0.067	
n63f	8	-0.016	0.151	13	+0.328	0.204	25	-0.114	0.238	6	-0.126	0.196	5	+0.134	0.175	41	+0.029	0.169	1	+0.363	
n63g	8	+0.040	0.242	13	+0.371	0.312	13	-0.138	0.259	6	-0.308	0.297	4	+0.073	0.291	21	+0.012	0.286	0		
n63h	8	-0.023	0.191	12	+0.145	0.261	22	-0.156	0.251	7	-0.203	0.260	4	-0.026	0.157	37	+0.004	0.177	1	+0.218	
n63i	8	-0.109	0.186	13	+0.191	0.175	25	-0.112	0.256	6	-0.317	0.119	5	-0.031	0.174	41	-0.015	0.160	1	+0.020	
n63l	8	-0.112	0.178	12	+0.184	0.194	22	-0.159	0.235	7	-0.169	0.194	5	+0.137	0.106	39	+0.013	0.155	1	+0.109	
n63m	8	+0.004	0.179	13	+0.357	0.168	13	-0.098	0.172	6	-0.187	0.182	4	-0.044	0.174	40	+0.049	0.231	1	+0.208	
n63n	8	-0.001	0.096	13	+0.297	0.201	21	-0.191	0.232	7	-0.288	0.183	5	-0.019	0.163	37	+0.047	0.219	1	+0.096	
l63p001	2	+0.003	0.012				1	-0.037		0						12	+0.066	0.104	0		
l63p002	2	-0.017	0.017				1	-0.126		0						12	+0.051	0.057	0		
l63p003	2	-0.122	0.071				1	+0.256		0						8	+0.019	0.100	0		
l63p004	2	-0.066	0.007				1	-0.487		0						10	-0.068	0.093	0		
l63p006	2	-0.044	0.014				1	+0.080		0						10	+0.028	0.152	0		

**Table A.4.** Neutron-capture abundances.

Star	nr	[Y/Fe] <sub>I</sub>	rms	nr	[Zr/Fe] <sub>II</sub>	rms	nr	[La/Fe] <sub>II</sub>	rms	nr	[Ce/Fe] <sub>II</sub>	rms	nr	[Nd/Fe] <sub>II</sub>	rms	nr	[Eu/Fe] <sub>II</sub>	rms
n63a	2	-0.680	0.134	0			2	+0.047	0.040	1	-0.365		3	+0.070	0.082	2	+0.238	0.064
n63b	1	-0.300		1			2	+0.214	0.022	0			3	+0.003	0.066	0		
n63c	2	-0.424	0.018	1	-0.280		2	+0.173	0.044	1	-0.285		3	+0.012	0.157	2	+0.283	0.020
n63d	2	-0.340	0.221	1	-0.205		2	+0.174	0.018	1	-0.323		3	+0.029	0.203	2	+0.288	0.168
n63e	2	-0.287	0.202	1	+0.133		2	+0.094	0.175	1	-0.169		3	+0.111	0.013	2	+0.260	0.035
n63f	2	-0.237	0.129	1	+0.091		2	+0.147	0.066	1	-0.233		3	+0.183	0.059	2	+0.265	0.000
n63g	0			1	-0.371		2	+0.238	0.279	1	-0.260		0			2	+0.267	0.161
n63h	2	-0.166	0.035	1	-0.066		2	+0.149	0.027	1	-0.341		3	-0.123	0.099	2	+0.183	0.013
n63i	2	-0.173	0.216	1	-0.228		2	+0.122	0.155	1	-0.290		3	-0.024	0.210	2	+0.202	0.071
n63l	2	-0.594	0.071	1	-0.071		2	+0.145	0.053	1	-0.289		3	+0.000	0.200	2	+0.233	0.108
n63m	2	-0.070	0.115	1	-0.395		2	+0.273	0.115	1	-0.325		3	+0.102	0.179	2	+0.305	0.025
n63n	2	-0.281	0.257	1	-0.464		2	+0.088	0.009	1	-0.364		3	-0.010	0.133	2	+0.257	0.084

**Table A.5.** [Zr/Fe]<sub>I</sub> and [Ba/Fe]<sub>II</sub> abundances.

Star	nr	[Zr/Fe] <sub>I</sub>	rms	nr	[Ba/Fe] <sub>II</sub>	rms
n63a	4	-0.337	0.113	3	-0.478	0.025
n63b	0			0		
n63c	4	+0.008	0.252	3	+0.016	0.149
n63d	6	-0.091	0.275	3	-0.214	0.071
n63e	4	-0.054	0.222	3	-0.083	0.069
n63f	3	-0.008	0.029	3	-0.036	0.102
n63g	0			3	+0.049	0.221
n63h	4	-0.094	0.228	3	-0.031	0.098
n63i	3	-0.094	0.063	3	+0.049	0.059
n63l	3	-0.149	0.038	3	-0.148	0.045
n63m	3	-0.122	0.280	3	+0.011	0.082
n63n	4	-0.068	0.162	3	-0.061	0.322
163p001	4	-0.013	0.127	1	+0.129	
163p002	4	-0.141	0.170	1	-0.091	
163p003	0			1	-0.077	
163p004	3	-0.116	0.197	1	-0.035	
163p006	1	-0.066		1	+0.136	

## **Appendix B: References for studies listed in Figures 11, 15, 20, and 21**

In Figures 11, 15, 20, and 21 we compare the average abundance ratios derived in NGC 6388 for some species to a sample of GCs and field stars, both in the disc and in the bulge, from a number of studies. Not all the elements were available for GC stars, whereas all species were sampled in the abundance analyses of comparison field stars in the Milky Way.

The GCs in our FLAMES survey, ordered by increasing metallicity, are listed in Table B.1 (we give the  $[Fe/H]$  value from UVES spectra used in the plots, from Carretta et al. 2009c or from individual papers, in parentheses). We note that some elements were analysed in the same study for many GCs, whereas other elements were obtained in the individual papers.

To GCs homogeneously analysed in our FLAMES survey (or with similar procedures), we added four metal-rich GCs from the same group of investigators (see Table B.2). For field Milky Way stars (in halo, disc, or bulge components), we used many studies, as detailed in the same table.

**Table B.1.** Globular cluster in our FLAMES survey: Elements and references.

GC and [Fe/H]	Ref for [Fe/H]	Ref for Mg, Si	Ref for Ca	Ref for other elem.	Other elements
NGC 7099 (M 30, -2.344)	Carretta et al. 2009c	Carretta et al. 2009a	Carretta et al. 2010b		
NGC 7078 (M 15, -2.320)	Carretta et al. 2009c	Carretta et al. 2009a	Carretta et al. 2010b		
Terzan 8 (-2.270)	Carretta et al. 2014a	Carretta et al. 2014a	Carretta et al. 2014a	Carretta et al. 2014a	Ti I, Cr, Mn, Ni, Y II, Ba, Nd
NGC 4590 (M 68, -2.265)	Carretta et al. 2009c	Carretta et al. 2009a	Carretta et al. 2010b		
NGC 4833 (-2.020)	Carretta et al. 2014b	Carretta et al. 2014b	Carretta et al. 2014b	Carretta et al. 2014b	Ti I, Cr, Mn, Ni, Y II, Y II, Ba, Nd
NGC 6397 (-1.988)	Carretta et al. 2009c	Carretta et al. 2009a	Carretta et al. 2010b	James et al. 2004a	Y II, Ba, Eu
NGC 6535 (-1.952)	Bragaglia et al. 2017	Bragaglia et al. 2017	Bragaglia et al. 2017	Bragaglia et al. 2017	Ti I, Cr, Mn, Ni
NGC 6809 (M 55, -1.934)	Carretta et al. 2009c	Carretta et al. 2009a	Carretta et al. 2010b		
NGC 5634 (-1.867)	Carretta et al. 2017	Carretta et al. 2017	Carretta et al. 2017	Carretta et al. 2017	Ti I, Cr, Mn, Co, Ni, Y II, Ba, La, Nd, Eu
NGC 6093 (M 80, -1.790)	Carretta et al. 2015	Carretta et al. 2015	Carretta et al. 2015	Carretta et al. 2015	Ti I, Cr, Mn, Co, Ni, Y II, Ba, La, Ce, Nd, Eu
NGC 1904 (M 79, -1.579)	Carretta et al. 2009c	Carretta et al. 2009a	Carretta et al. 2010b		
NGC 6254 (M 10, -1.575)	Carretta et al. 2009c	Carretta et al. 2009a	Carretta et al. 2010b		
NGC 6752 (-1.555)	Carretta et al. 2009c	Carretta et al. 2009a	Carretta et al. 2010b	James et al. 2004b	Y II, Ba, Eu
NGC 3201 (-1.512)	Carretta et al. 2009c	Carretta et al. 2009a	Carretta et al. 2010b		
NGC 6715 (M 54, -1.510)	Carretta et al. 2010c	Carretta et al. 2010c	Carretta et al. 2010c	Carretta et al. 2010c	Ti I, Cr, Mn, Co, Ni
NGC 5904 (M 5, -1.340)	Carretta et al. 2009c	Carretta et al. 2009a	Carretta et al. 2010b		
NGC 6218 (M 12, -1.330)	Carretta et al. 2009c	Carretta et al. 2009a	Carretta et al. 2010b		
NGC 288 (-1.305)	Carretta et al. 2009c	Carretta et al. 2009a	Carretta et al. 2010b		
NGC 1851 (-1.180)	Carretta et al. 2011	Carretta et al. 2011	Carretta et al. 2011	Carretta et al. 2011	Ti I, Cr, Mn, Co, Ni, Y II, Zr II, Ba, La, Nd, Eu
NGC 362 (-1.170)	Carretta et al. 2013	Carretta et al. 2013	Carretta et al. 2013	Carretta et al. 2013	Ti I, Cr, Mn, Co, Ni, Y II, Zr II, Ba, La, Nd, Eu
NGC 6121 (M 4, (-1.168)	Carretta et al. 2009c	Carretta et al. 2009a	Carretta et al. 2010b		
NGC 2808 (-1.130)	Carretta 2015	Carretta 2015	Carretta 2015	Carretta 2015	Ti I, Cr, Mn, Ni
NGC 6171 (M 107, -1.033)	Carretta et al. 2009c	Carretta et al. 2009a	Carretta et al. 2010b		
NGC 6838 (M 71, -0.832)	Carretta et al. 2009c	Carretta et al. 2009a	Carretta et al. 2010b		
NGC 104 (47 Tuc, -0.768)	Carretta et al. 2009c	Carretta et al. 2009a	Carretta et al. 2010b	Carretta et al. 2004 James et al. 2004a	Cr, Mn, Ni; Y II, Ba, Eu
NGC 6388 (-0.480)	Carretta&Bragaglia 2022a	this work	this work	this work	Ti I, Cr I, Mn, Co, Ni, Y I, Zr sc I, Ba, La, Ce, Nd, Eu
NGC 6441 (-0.430)	Carretta et al. 2009c	Gratton et al. 2006	Gratton et al. 2006	Gratton et al. 2006	Ti I, Cr, Mn, Ni, Y I, Zr I, Ba, Eu

**Table B.2.** Literature data: Elements and references.

GC or system	Reference	elements
NGC 6440 ([Fe/H]= -0.50)	Muñoz et al. 2017	Mg, Si, Ca, Sc, Ti, Mn, Ni, Co, Ba, Eu
NGC 5927 ([Fe/H]= -0.47)	Mura-Guzmán et al. 2018	Mg, Si, Ca, Sc, Ti, V, Cr, Mn, Co, Ni, Y, Zr, Ce, Ba, Eu
NGC 6528 ([Fe/H]= -0.20)	Muñoz et al. 2018	Mg, Si, Ca, Sc, Ti, V, Cr, Mn, Co, Ni, Zr, Ba, Eu
NGC 6553 [Fe/H]= -0.14)	Muñoz et al. 2020	Mg, Si, Ca, Sc, Ti, V, Cr, Mn, Ni, Y, Zr, Ce, Ba, Eu
halo/disc	Adibekyan et al. 2012	Ca
	Battistini and Bensby 2016	Zr, La, Ce, Nd
	Beirão et al. 2005	Mg
	Bensby et al. 2014	Mg, Ca, Cr, Ni, Y, Ba
	Brewer et al. 2016	Mg, Mn, Ni, Y
	Delgado Mena et al. 2017	Si
	Gratton et al. 2003	Mg, Si, Ca, Ti, Cr, Mn, Ni
	Ishigaki et al. 2012, 2013	Mg, Si, Ca, Ti, Cr, Mn, Co, Ni, Y, Zr, Ba, La, Nd, Eu
	Lai et al. 2008	Si
	Neves et al. 2009	Mg, Si, Ti, Cr, Mn, Co, Ni
	Reddy et al. 2003	Si
	Reddy et al. 2006	Ca
	Reggiani et al. 2017	Mg, Cr, Mn, Co, Ni, Y, Zr, Ba
	Roederer et al. 2014.	Si, Ca, Ti, Cr, Mn, Co, Ni, Y, Zr, Ba, La, Ce, Nd, Eu
bulge	Alves-Brito et al. 2010	Mg, Ca, Ti
	Barbuy et al. 2013	Mn
	Bensby et al. 2017	Mg, Si, Ca, Ti, Cr, Ni, Y, Ba
	da Silveira et al. 2018	Mg, Si, Ca
	Duong et al. 2019a	Ti
	Duong et al. 2019b	Cr, Mn, Co, Ni, Zr, La, Nd, Eu
	Forsberg et al. 2019	Zr, La, Ce, Eu
	Johnson et al. 2014	Mg, Si, Ca, Cr, Co, Ni
	Jönsson et al. 2017	Mg, Ca, Ti
	Lomaeva et al. 2019	Cr, Mn, Co, Ni
	Lucey et al. 2019	Mg, Si, Ca, Ti, Cr, Mn, Co, Ni, Y, Zr, Ba, La, Nd, Eu
	Lucey et al. 2022	Ti